Femtosecond optical bit multiplication by photon echoes excited with spectrally modulated laser pulses

Diploma thesis made by:
Cecilia Nilsson

Performed at the Physical Chemistry Institute at the ETH in Zürich, Switzerland during the winter semester 1996/97

Lund Reports on Atomic Physics, LRAP-213

ACKNOWLEDGEMENTS

I would like to thank the following people for helping me to do my diploma thesis at ETH and for their support during that time.

First of all I would like to thank Professor Wild for giving me the opportunity to do my diploma thesis in his group at ETH in Zürich.

Professor Sune Svanberg for wakening my interest for two pulse photon echo in his course "Atom och molekylspektroskopi" and for helping me to find a university abroad where I could do my diploma thesis in this field.

The leader of the sub-group in time domain holography, Professor Aleksander Rebane for letting me do my diploma thesis in this group, for suggesting the subject of spectrally modulated photon echoes for my diploma thesis and for interesting and enlightening theoretical talks and proof-reading.

To my examiner Docent Stefan Kröll for his support, especially for helping me to arrange to do my diploma thesis in Professor Wilds group at ETH, Zürich, for the theoretical discussions and for proof-reading.

To Jürgen Gallus. For his very instructive and helpful explanations of the laser system, the experimental setup and theory. But also for his patience with my German and his practical jokes.

Daniel Erni for explaining both theory and the real practical laboratory work in a very comprehensible way. But also for the immense amount of work he has put in proof-reading this report.

Olavi Ollikainen for help during the experiments and explanations of the two pulse photon echo theory.

Vitaly Krylov for help with the laboratory work.

Ernst Udo Wallenborn for long and profitable quantum mechanical discussions.

Daniel Reiss for helping me with the authorities.

All the rest in the Wild-group, for your friendliness, helpfulness and patience with my German.

To my parents. For all the love, encouragement and support that you've given me. This empowered me to start my studies in engineering physics, which are completed with this diploma thesis.

To my boyfriend for coming with me to Switzerland and always being there for me.

TABLE OF CONTENTS

Acknowledgements i

Table of Contents iii

Summary v

Zusammenfassung viii

1 Introduction 1

2 The femtosecond laser system 2

2.1 The Titanium:Sapphire oscillator 2

2.2 The pulse stretcher 7

2.3 The amplifier 8

2.4 The pulse compressor 10

3 Spectral-domain shaping of femtosecond laser pulses 12

3.1 Spectral modulation setup 12

3.2 Spatial light modulators (SLM) 14

3.2.1 Mechanical amplitude masks 14

3.2.2 Liquid Crystal Array (LCA) 15

4 Femtosecond two pulse photon echo 20

4.1 Theory 20

4.1.1 Density matrix formalism 20

4.1.2 Bloch vector formalism 36

4.1.3 π- and $\pi/2$-pulse excitation 40

4.1.4 Two pulse photon echo 42

4.2 Experiment 47

4.2.1 Modulation of one excitation pulse 47
4.2.2 Modulation of both excitation pulses 48
4.2.3 Experimental details 49
5 Results and discussion 53
5.1 The echo intensity dependence of the time delay between the excitation pulses 53
5.2 Modulation of one excitation pulse using an LCA 53
5.3 Modulation of both excitation pulses using two bar masks 55
5.4 Temporal measurements of spectrally modulated photon echoes . 57
5.5 Discussion of error sources 60
6 Conclusions 62
6.1 Bit multiplication in the spectral-domain 62
6.2 Future applications 64
7 References 65

SUMMARY

The goal of the present work was to study the spectral and temporal properties of photon echoes excited in dye-doped polymer films at liquid-helium temperatures, by spectrally modulated ultrashort pulses.

In the cases of moderate excitation intensities, the two pulse photon echo's, (2PPE) spectral intensity, $I_e(\omega)$, can be expressed as:

$$I_e(\omega) \sim I_1(\omega) \cdot I_2^2(\omega)$$

where $I_1(\omega)$ and $I_2(\omega)$ are the intensity spectrum component of the first and the second excitation pulse. According to this formula, the echo spectrum can be viewed as a direct multiplication of two input information bit vectors, A_i^{IN1} and A_i^{IN2}, coded into the spectra of the excitation pulses.

$$A_i^{OUT} = A_i^{IN1} \cdot A_i^{IN2} \tag{0.1}$$

where A_i is the i^{th} bit of the output or the input vector. The upper index OUT, correspond to the output vector, the echo, and the indexes IN1 and IN2 to the temporal order of the input vectors, the excitation pulses. The bits, A_i, can have the values 0 or 1. The coding algorithm can be of the form:

$$A_i = \begin{cases} 1 \text{ when } I_e(\omega_i) \geq I_0 \\ 0 \text{ when } I_e(\omega_i) < I_0 \end{cases}$$

for a suitable threshold intensity I_0, see figure 0.1.

In this work we have studied the potential of spectral domain processing by 2PPE. We have performed 2PPE experiments with spectrally modulated excitation pulses and demonstrated that the echospectra correspond to the product of the input information.

To demonstrate the validity of equation (0.1), we have performed experiments where the spectrum of the photon echo's excitation pulses was modulated by

using a special setup consisting of a pair of diffraction gratings and a spatial light modulator.

The laser system we use is a regeneratively-amplified Titanium:Sapphire laser, CPA 1000 (Clark MXR), which generates pulse lengths of about 100 fs at a repetition rate of 1 kHz and with a pulse energy of circa 1 mJ. Since the pulses are that short in the temporal domain, their spectral width is in the order of 10 nm. By using a grating pulse shaper setup, we can diffract the different frequency components of the pulse at different angles. This transforms the pulse from the temporal domain into the spectral domain. In the spectral domain we can cancel certain frequency components, and thereby code the input information directly into the spectra of the excitation pulses, $E_1(\omega)$ and $E_2(\omega)$. We have constructed a special modulation setup, where both pulses passes through two equivalent but spatially separated beam paths in the same modulator, so that both of them are spectrally modulated independently of each other by two different amplitude masks. The two modulated excitation pulses are hereafter directed onto a sample, which consists of a thin polyvinylbutyral film, doped with molecules of a zinc-naphthalocyanine dye and cooled to the temperature $T = 2$ K in a liquid helium cryostat. The sample responds to the excitation by emitting an echo at the time τ after the second excitation pulse, where τ corresponds to the time between the first and the second excitation pulse. The echo is emitted, in the direction: $\vec{k}_e = 2 \cdot \vec{k}_2 - \vec{k}_1$, where $\vec{k}_1$ and $\vec{k}_2$ corresponds to the direction of the first and the second excitation beam, respectively.

Figure 0.1 shows the result, where we perform spectral multiplication. The input vectors, A^{IN1} and A^{IN2}, are coded into the intensity spectrum of the first, $I_1(\omega)$, and second excitation pulse, $I_2(\omega)$, respectively. The product, $A_i^{OUT} = A_i^{IN1} \cdot A_i^{IN2}$ appears as the intensity spectrum, $I_e(\omega)$, of the echo signal measured with a monochromator. This result shows that we are able to carry out femtosecond time scale multiplication of the input information coded into the excitation spectra.

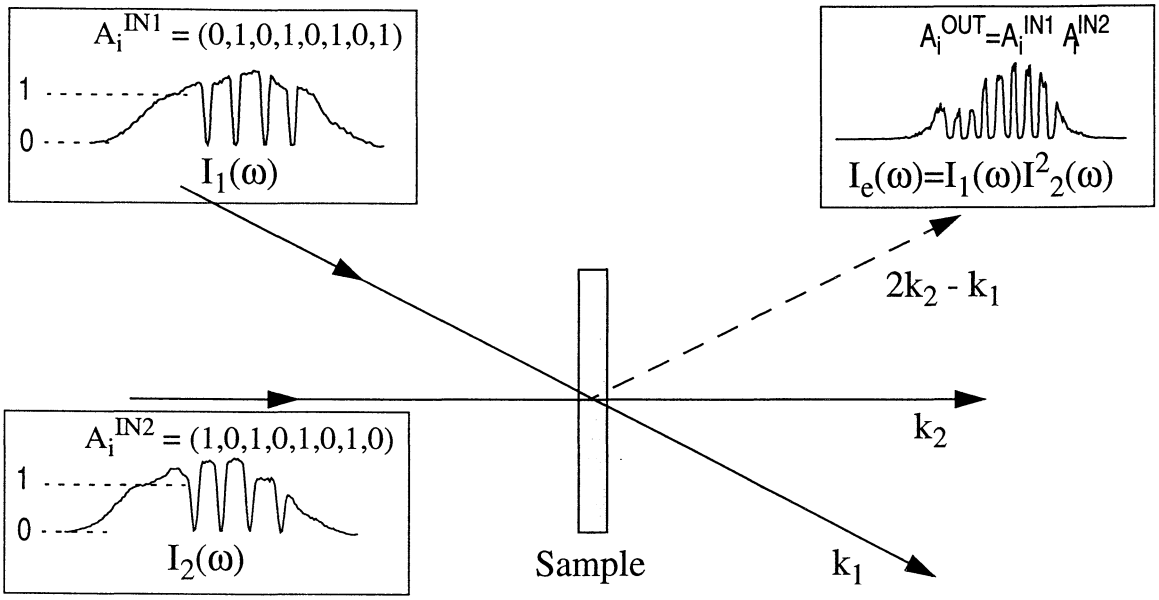

Figure 0.1: Spectral multiplication by femtosecond 2PPE.

In addition, we investigated the intensity dependence of the echo spectrum in order to estimate the suitable intensity range, for which equation (0.1) is valid. As a result, we observed that for high excitation intensities the echo spectrum does no longer correspond to the pure multiplication of the excitation spectra. Nevertheless, data processing can still be achieved by choosing the threshold level more carefully.

The excitation and echo signal was detected time resolved and compared with numerical simulation. For the spectral modulation performed with the liquid crystal array, only the time traces of the excitation pulses were measured and for these were only a good agreement obtained if the proper phase shift was included in the simulation.

ZUSAMMENFASSUNG

Ziel dieser Arbeit war, das zeitlichen und spektrale Verhalten von mit spektral modulierten ultrakurzen Laserpulsen in einem farbstoff-dotierten Polymerfilm bei flüssig-Helium-Temperatur erzeugten Zweipuls-Photonechos zu untersuchen.

Bei mittleren Anregungsintensitäten lässt sich die spektrale Intensität des Zwei-Puls-Photonechos $I_e(\omega)$ durch folgenden Ausdruck beschreiben:

$$I_e(\omega) \sim I_1(\omega) \cdot I_2^2(\omega),$$

wobei $I_1(\omega)$ und $I_2(\omega)$ die Intensitäten der spektralen Komponenten des ersten und zweiten Anregungspulses sind. Das Spektrum des Echos kann daher als eine direkte Multiplikation zweier Input-Vektoren dargestellt werden, die als Intensitätsverteilung in den Spektren der Anregungspulse codiert sind.

$$A_i^{OUT} = A_i^{IN1} \cdot A_i^{IN2} \tag{0.2}$$

Hierbei ist A_i die i-te Vektorkomponente des jeweiligen Input- bzw. Output-Vektors. Der Index OUT bezeichnet den Output-Vektor (im Experiment das Echo), und IN1 und IN2 entsprechen der zeitlichen Ordnung der Input-Vektoren (im Experiment den Anregungspulsen). Die Bits A_i haben den Wert 0 oder 1. Der codierte Algorithmus kann in der folgenden Form beschreiben werden:

$$A_i = \begin{cases} 1 \text{ für } I_e(\omega_i) \geq I_0 \\ 0 \text{ für } I_e(\omega_i) < I_0 \end{cases}$$

für einen geeigneten Schwellenwert I_0 (Figur 0.2).

In dieser Arbeit haben wir Möglichkeiten der Informationsverarbeitung mittels 2PPE auf spektraler Ebene untersucht. Wir haben 2PPE Experimente mit spektral modulierten Anregungspulsen durchgeführt und gezeigt, dass die im Spektrum des Echos codierte Information dem Produkt der Input-Informationen entspricht.

Um die Gültigkeit der Gleichung (0.2) zu demonstrieren, haben wir Experimente durchgeführt, in denen Spektren der Anregungspulse des Photonechos mittels eines speziellen Aufbaus, bestehend aus zwei Diffraktionsgittern und einem räumlichen Lichtmodulator (SLM), spektral moduliert werden können.

Für unsere Experimente haben wir einen regenerativ verstärkten Ti:Sp Laser - CPA 1000 (Clark MXR)- benutzt, der mit einer Repetitionsrate von 1 kHz Pulslängen von ungefähr 100 fs mit einer Pulsenergie von circa 1 mJ erzeugt. Pulse dieser länge haben eine spektrale Halbwertsbreite von etwa 10 nm. Durch Beugung dieser Pulse an einem Gitter können wir das Pulsspektrum räumlich auffächern, was einer Transformation von der zeitlichen in die spektrale Domäne entspricht. Im spektralen Bereich können wir nun beliebige Frequenzkomponenten auslöschen, und dadurch die Input-Information direkt in den Spektren $E_1(\omega)$ und $E_2(\omega)$ der Anregungspulse codieren.

Zur spektralen Modulation der Anregungspulse haben wir einen Aufbau konstruiert, welchen beide Pulse auf zwei äquivalenten, aber räumlich getrennten Wegen passieren, sodas beide unabhängig voneinander mit zwei verschiedenen Amplitudenmasken moduliert werden können. Die beiden modulierten Anregungspulse schickt man danach zeitverschoben auf einen Polyvinylbutyral-Film der mit einem Zink-Naphthalocyanin-Farbstoff dotiert und in einem Kryostaten in superflüssigem Helium auf einer Temperatur von 2 Kelvin abgekühlt ist. Die Probe reagiert auf die Anregung durch Emittieren eines Echos im zeitlichen Abstand τ zum zweiten Anregungspuls, wobei τ der Zeitabstand zwischen dem ersten und zweiten Anregungspuls ist. Sind $\vec{k}_1$ und $\vec{k}_2$ die Richtungsvektoren der beiden Anregungspulse, so wird das Echo in Richtung $\vec{k}_e = 2 \cdot \vec{k}_2 - \vec{k}_1$ emittiert.

Figur 0.2 zeigt, wie wir die spektrale Multiplikation ausführen, und das entsprechende Echospektrum. Die Inputvektoren A^{IN1} und A^{IN2} sind in den Intensitätspektren des ersten,$(I_1(\omega))$ bzw. zweiten $(I_2(\omega))$ Anregungspulses codiert. Das Produkt, $A_i^{OUT} = A_i^{IN1} \cdot A_i^{IN2}$ zeigt sich im Intensitätsspektrum $I_e(\omega)$ (gemessen mit einem Monochromator) vom Echosignal. Dieses Resultat zeigt, dass wir eine Multiplikation der Input-Information, die in den Anregungsspektren codiert ist, in einer Femtosekunden-Zeitskala durchführen können.

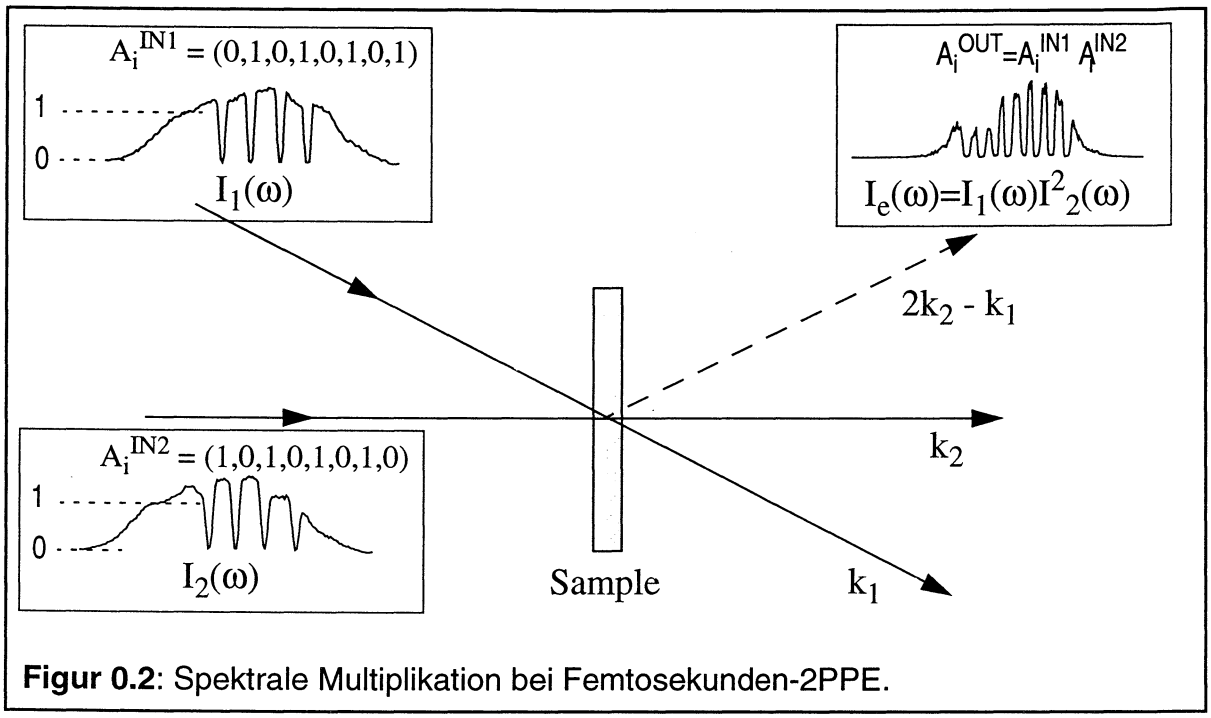

Figur 0.2: Spektrale Multiplikation bei Femtosekunden-2PPE.

Ausserdem haben wir die Intensitätsabhängigkeit des Echospektrums von den Anregungspulsen untersucht, um den Intensitätsbereich, in dem Gleichung (0.2) erfüllt ist, abzuschätzen. Dabei haben wir beobachtet, dass das Spektrum des Echos bei höheren Anregungsintensitäten nicht mehr einer reinen Multiplikation der Anregungsspektren entspricht. Durch eine geeignetere Wahl des Schwellenwerts I_0 ist aber immernoch Informationsverarbeitung auf dieselbe Art möglich.

Auch die Zeitantworten der Anregungs- und Echopulse wurden detektiert und mit einer numerischen Simulation verglichen. Für die spektralen Modulationen, die mit einem Flüssigkristall-Array (LCA) ausgeführt wurden, wurden nur die Zeitsignale der Anregungspulse aufgenommen. Unter Berücksichtigung eines inhärenten Phasenshifts des LCA's erhielt man eine sehr gute Übereinstimmung dieser Zeitsignale mit den Simulationen.

1 INTRODUCTION

The idea for the experimental setup to my diploma thesis was given by Professor Aleksander Rebane, at the laboratory of Physical Chemistry at ETH in Zurich. The experiment continues the work performed by Jürgen Gallus in his diploma thesis, [GAL-96]. The experiments contain spectral modulations of pulses with a duration of about 100 fs. Since the laser pulses are that short, their spectra are as broad as 10 nm, which make them very suitable for spectral modulations. A grating and lens setup is used to transform the pulse out of the temporal domain and into the spectral domain. The grating diffracts the different frequency components in the pulse at different angles, whereby making the different colours in the pulse spatially separated. By blocking certain frequency components, the pulse's spectral and temporal appearances are changed. A sample with an inhomogeneously broadened absorption band is then exposed to the two excitation pulses separated by the time τ. The sample answers by emitting an echo pulse at the time τ after that the second excitation beam has hit the sample.

My task was to investigate the photon echo experimentally, if it is excited by two pulses which have certain frequency components that overlap and some that do not overlap, (figure 1.1.) The question to be answered in my diploma thesis was: "Do the spectra of the echoes only consist of the spectral components that exist in both pulses?"

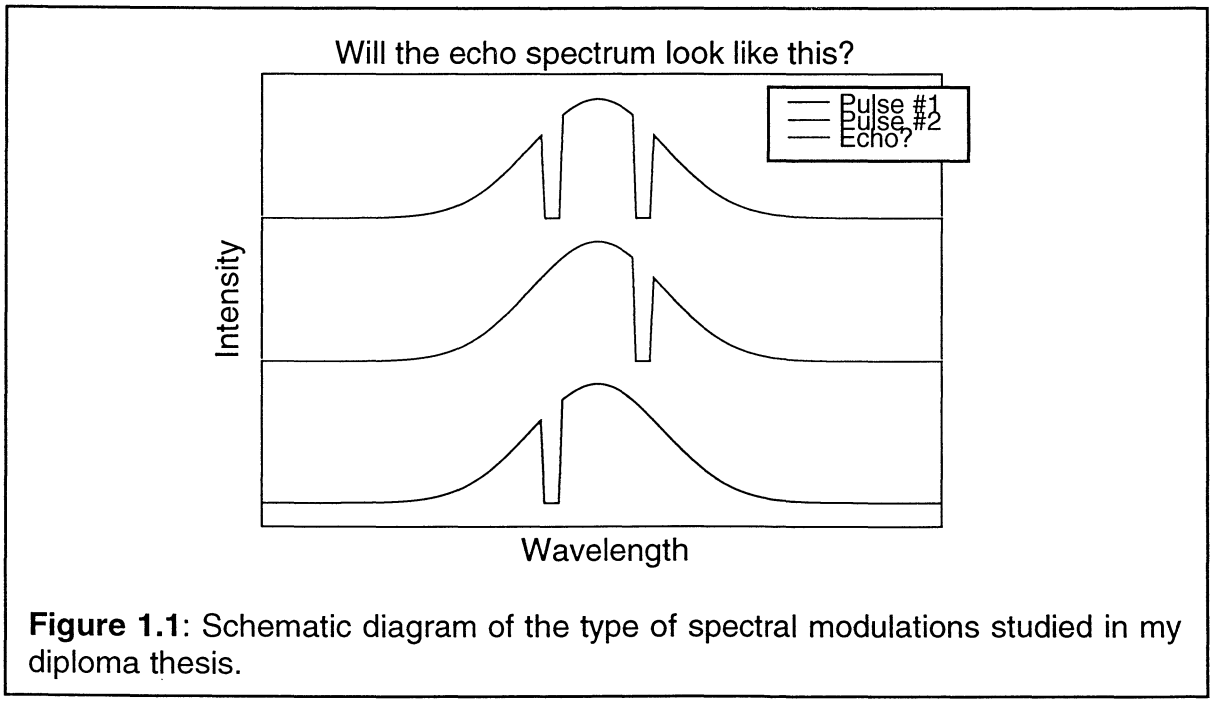

Figure 1.1: Schematic diagram of the type of spectral modulations studied in my diploma thesis.

2 THE FEMTOSECOND LASER SYSTEM

The laser system consists of a femtosecond oscillator and a regenerative amplifier. In order to amplify the short pulses, they have to be stretched out in time before coupling them into the amplifier cavity. Finally, the chirped pulses are recompressed in a compressor stage.

2.1 THE TITANIUM:SAPPHIRE OSCILLATOR

In the femtosecond oscillator, a 20 mm long and 4 mm thick Sapphire crystal, doped with Ti^{3+} ions (Ti:S) is pumped by an argon ion laser. The energy level diagram for the Ar^{+}-laser, is shown in figure 2.1. The ionisation (a) of the argon atom, and the excitation (b) of the argon ion, occurs through a gas discharge. The electronic configurations, $3s3p^{5}4p$ and $3s3p^{5}4s$, are in reality separated into terms, which allows different transitions in the visible range. The strongest transitions are at 488 nm (blue-green) and 514,5 nm (green). The all-line continuous (cw) output beam of the argon laser is focused on the Ti:S crystal (e). The crystal responds by emitting fluorescence radiation in the wavelength range of 670 to 1070 nm, with a peak at 800 nm (figure 2.1). There are two reasons for the broad, widely separated absorption and fluorescence bands. The strong coupling between the 3d-orbital of the Ti^{3+} ions and the Al_2O_3 host lattice and the different surroundings for every Ti^{3+} ion causes the inhomogeneous broadening of the emission, [KNE-95], [KOE-96]. In Ti:S crystals, hardly any self-absorption occurs within the emission range, which makes this gain medium superior to other tunable solid-state lasers.

The Ti:S crystal is colinearly pumped by the argon laser, through a curved dichroic mirror, with zero reflectance at the argon laser wavelengths, see figure 2.2. The fluorescence generated in the Ti:S crystal is then reflected back and forward in the cavity by two mirrors, one high reflecting end mirror, and one 5%-transmission output coupler. Free running, the resonator has two stable eigenmodes, a continuous wave (cw) mode and a pulsed mode, which spatially differs from each other. Two prisms are placed in the cavity in order to select the pulsed mode. The main purpose of the prisms is to reduce the group velocity dispersion. This is done by moving one of the prisms back and forward, so that the laser

pulse goes through more or less glass. The two prisms also work as spectral wavelength separators. The required wavelength range can be selected by changing the position and the size of a slit, which is placed between the second prism and the end mirror, see figure 2.2.

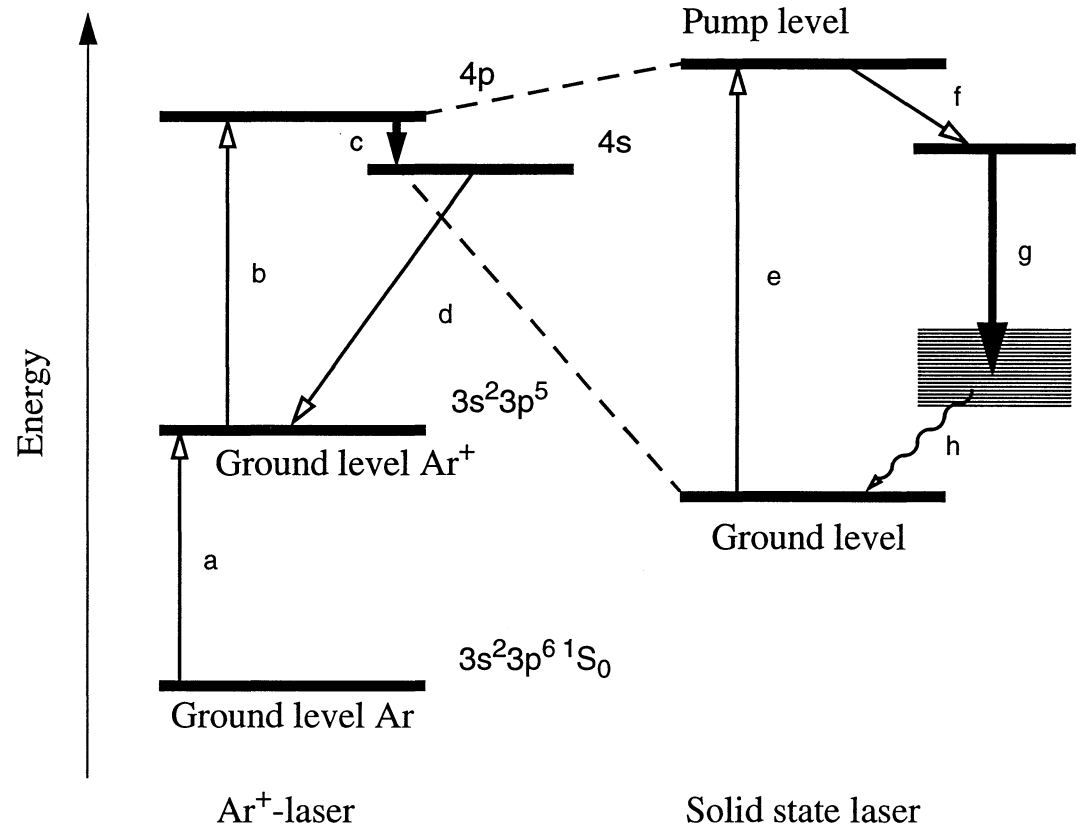

Figure 2.1: The energy level diagram for an argon ion laser (left), and a solid state laser e.g. the Titanium:Sapphire (right, schematic).

The fast, additional, saturable absorber, usually needed as an additional component in order to achieve the pulsed mode is not necessary here. The pulsed mode is instead obtained by a combination of the nonlinear Kerr effect in the Titanium:Sapphire crystal, and mode losses introduced by a spatial mask, here the mechanical slit. In the crystal, the electric field of the beam creates a polarization in the electron orbitals of the ions. Because the pulse in the resonator is very short and the curved mirrors focus the pulse onto a very small volume in the crystal, the peak intensity of the electric field are high (average power in the cavity: ~8 W, Repetition rate: 100 MHz, Energy per pulse: $8*10^{-8}$ J, Length of a pulse: ~70 fs, Maximum intensity: ~1 MW). Therefore is the refracting index of the crystal slightly changed by the Kerr effect every time the pulse passes through the crystal, forming a transient lens which focuses the beam. The part of the mode

that has the highest intensity, will therefore be more focused by the crystal and have a smaller diameter at the slit. Thus, it will experience lower losses, compared to the less intensive part of the mode at the slit. The pulse will this way be shortened by each passage through the cavity.

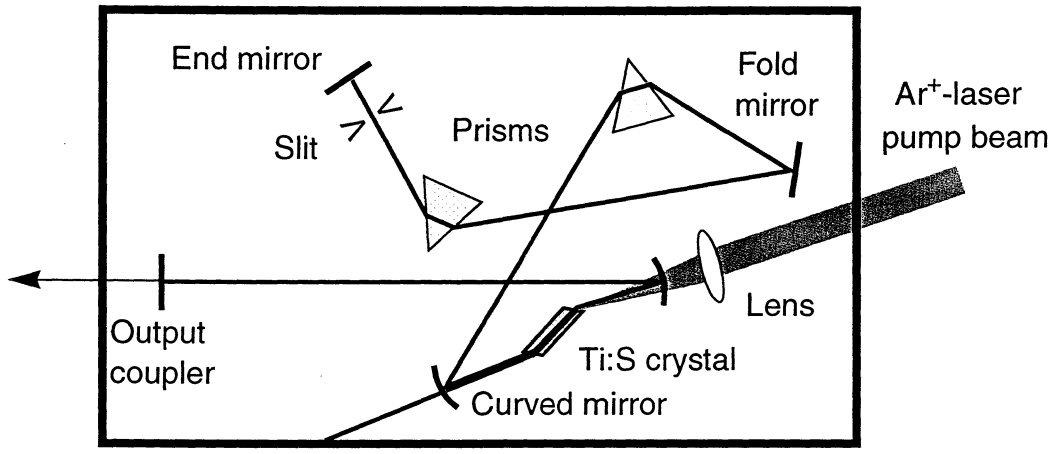

Figure 2.2: Setup of the fs-oscillator.

This so-called Kerr-lens mode-locking has two big advantages. Firstly, it is a passive mechanism: No acousto-optical modulators or similar active devices are needed. And secondly, the Kerr polarization of the crystal occurs at least a thousand times faster than the formation of molecular dipoles in dye liquids [SCH-94].

The output of the oscillator, is a pulse train with a repetition rate determined by the cavity length, according to $\Delta\nu = 2L/c$ (here $\Delta\nu = 100$ MHz which corresponds to a temporal spacing of 10 ns between each pulse). The spatial mode of the output is essentially a TEM_{00}, with three weaker side lobes, forming a triangle mode. The polarization of the beam is horizontal.

Pulse lengths down to $\Delta t = 70$ fs can be achieved with this laser system, Clark MXR, CPA 1000. Δt is measured at full width at half maximum (FWHM) of the autocorrelation trace, figure 2.3, under the assumption of a sech^2-intensity profile. Theoretically, this is an ideal shape for a passively mode locked pulse, in contrast to a gaussian pulse shape for a typical actively mode locked laser.

The time and frequency domain are related to each other by the Fourier transform. In consequence, the shorter a pulse is in the time domain, the broader its spectrum has to be. This fact is expressed by the time bandwidth product of the

pulse: $\Delta t \cdot \Delta \nu \sim$ const.. The value of the constant depends on the amplitude shape and phase of the pulse. It is equal to 0,31 for a I(t) ~ sech^2(t/dt) transform-limited pulse. Figure 2.3 shows the autocorrelation and the spectra of the oscillator pulse. The autocorrelation of a model sech^2-intensity profile is also plotted in the left graph in figure 2.3, which overlaps well with the experimental data. The pulse length is calculated to 73 fs and the spectral width is 12 nm, which yields a time bandwidth product of 0.45. This means that the oscillator pulse, at this central frequency, is not fully transform limited. At 780 nm, which the oscillator and the amplifier are optimized for, the pulse length is the same, but the spectral width is only 10 nm, giving rise to a bandwidth product of 0.35, [GAL-96]. The reason for working at this wavelength is that the absorption line of our sample is at 770 nm, and since the amplifier causes a shift of 5 nm to the red, due to the gain profile of the Ti:S crystal, we have to compensate for this shift.

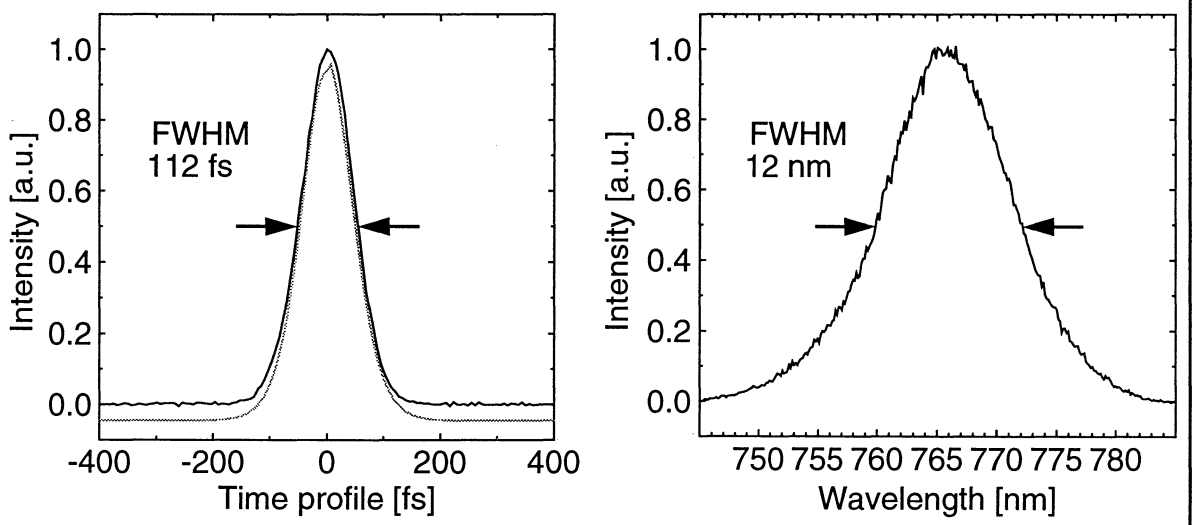

Figure 2.3: Autocorrelation (left) and its spectra (right) of the oscillator pulse.The dotted line is a sech^2 fit to the experimental data, yielding a FWHM of 73 fs. Because the fit so well corresponds to the measured signal, it has been lowered in the graph.

In the next step, the laser pulses from the oscillator are amplified. The use of a similar cavity as that of the oscillator for this purpose is not wise, because of the poor net gain of some percent that can be achieved. In addition, the peak intensity of ultrashort pulses are near the damage threshold of most of the optical elements anyhow. To overcome this disadvantage, the technique of "chirped pulses" is applied [MAI-88]. This concept means that the oscillator pulse is stretched out in time. The energy of the pulse is then spread out over a far longer time. Thus the peak intensity is lowered by the same inverse factor. This chirped pulse is ampli-

fied in another Ti:S gain crystal, and thereafter directed into the compressor which compresses the pulse length more or less back to its original length.

The optical setup for these three steps (stretching, amplification, compression) is optimally designed in a symmetric way, i.e. the output of each step is retroreflected into the same path as the input. This requires an optical switch that prevents the input into any component already passed by. This is achieved by an optical isolation system made up of two polarizing beamsplitters, a $\lambda/2$-plate and a Faraday-rotator. It is placed between the oscillator and the stretcher, see figure 2.4. The horizontally polarized light from the oscillator passes through the beamsplitter. The polarization is then turned $\pi/4$ rad by the $\lambda/2$-plate, but then turned back the same amount by the Faraday-rotator, so that the horizontally polarized light passes through the next beamsplitter and enters the stretcher. As the stretcher output is reflected into the same path, the beam passes through the second beamsplitter again and goes then the opposite way through the rotator and the $\lambda/2$-plate. This time the Farady rotator turns the polarization by $\pi/4$ rad, but now in the opposite direction as last time. By passing through the $\lambda/2$-plate, the total amount of rotation is now $\pi/2$ rad. This results in an output of vertically polarized light which is reflected by the beamsplitter towards the amplifier, thus prohibiting it to enter the oscillator again.

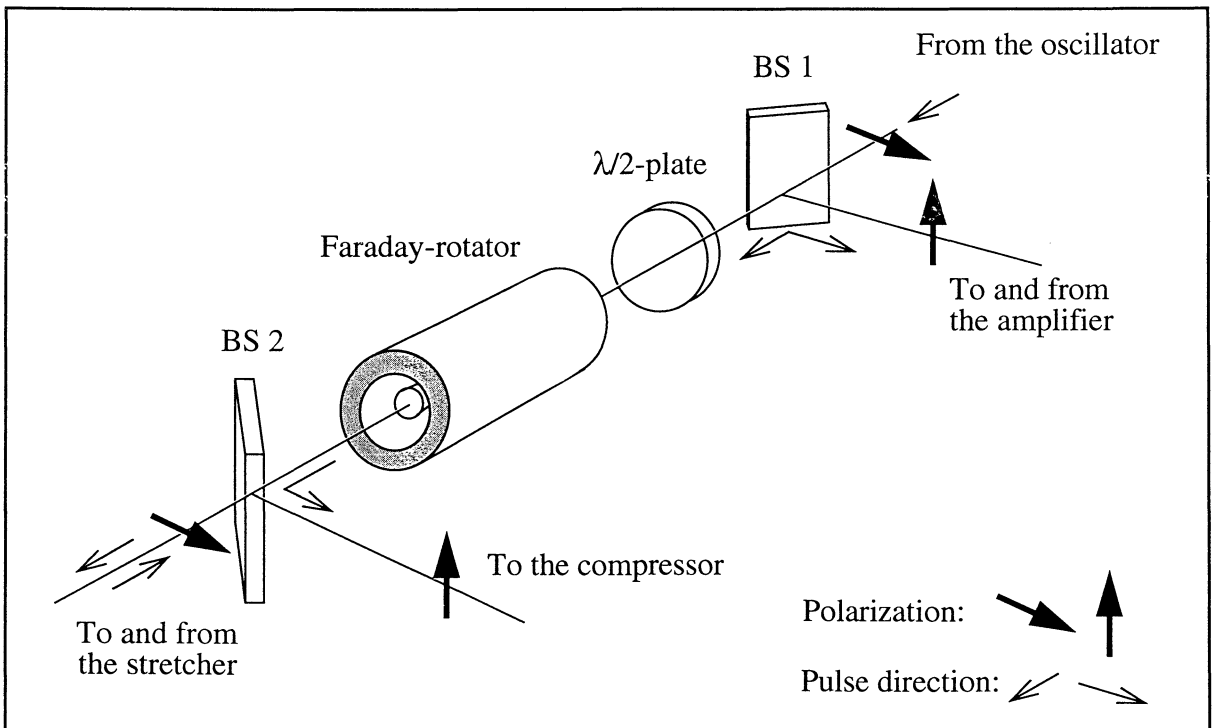

Figure 2.4: The optical isolator.

2.2 THE PULSE STRETCHER

After the pulse has passed through the optical isolator, a grating and mirror setup with positive group velocity dispersion stretches the pulse to a length that is about 2000 times longer than the oscillator pulse.

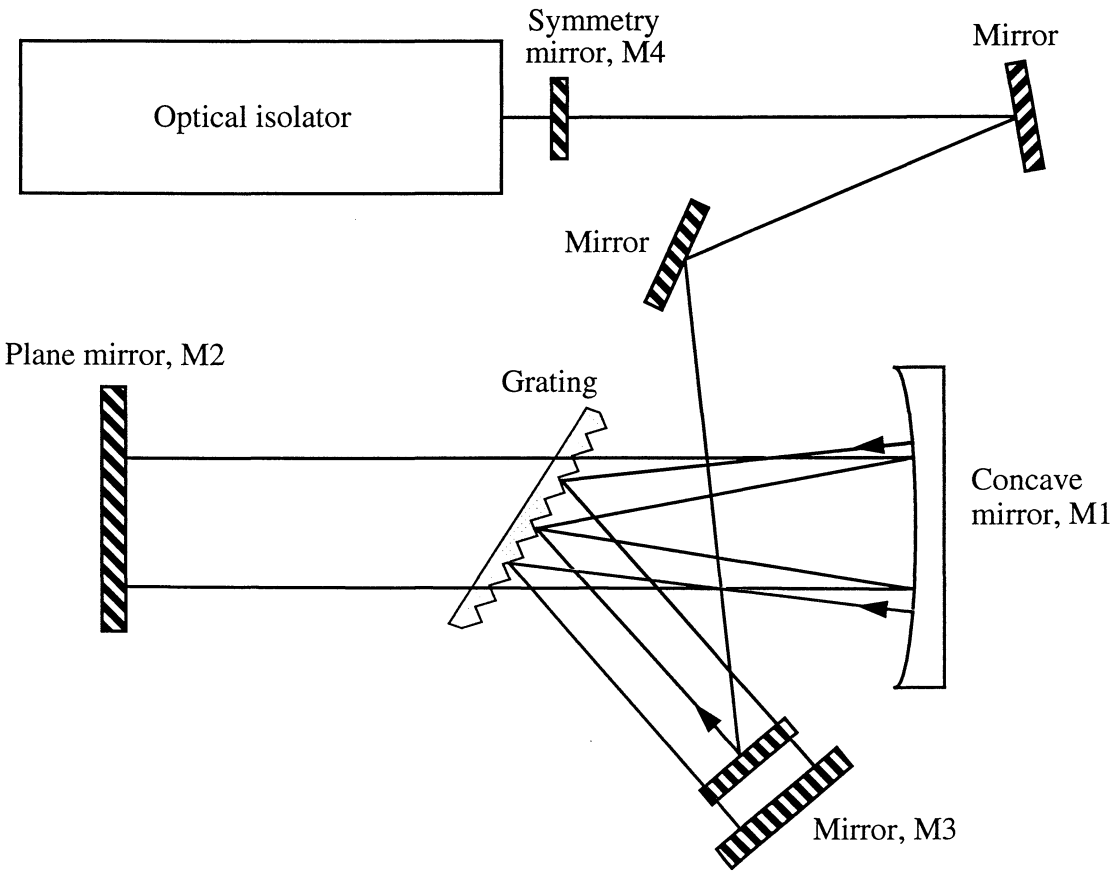

Figure 2.5: Schematic diagram of the pulse stretcher.

By a grating with 1400 lines per millimeter, the pulse is being angularly dispersed into its different frequency components, see figure 2.5. It's then reflected by a concave mirror, M1, towards a plane mirror, M2, placed in the focus of the concave mirror. This plane mirror reflects the pulse back on to the concave mirror and the grating. Because the grating is slanted in reference to the two mirrors, as shown in figure 2.5, the blue light travels a longer way then the red, so that the different colours return to the grating separated in time. That means that the pulse has been stretched out in time by its passage through the setup. The pulse then hits another mirror, M3, which reflects the pulse once again back through the

whole setup. Finally, the symmetry mirror M4 is hit, which reflects the pulse back again. So in total, the pulse is dispersed eight times by the grating. The result is a chirped pulse, circa 2000 times longer then when it left the oscillator. The pulse now passes through the optical isolator, whereby its polarization is changed to vertical, as described in chapter 2.1, and is reflected towards the amplifier.

2.3 THE AMPLIFIER

The gain medium of the amplifier is again a Titanium:Sapphire crystal. The design of the cavity is as simple as possible, only involving two curved mirrors. There are two reasons for that. The most important factor is the quality of the spatial mode of the amplified pulse, which is determined by the cavity. Since we have an extreme nonlinear amplification, any spatial and/or spectral irregularity in the pulse would increase further and become more pronounced. Secondly, once the oscillator pulse is coupled into the amplifier cavity, no complicated adjustments are needed to optimize the amplification of the pulse.

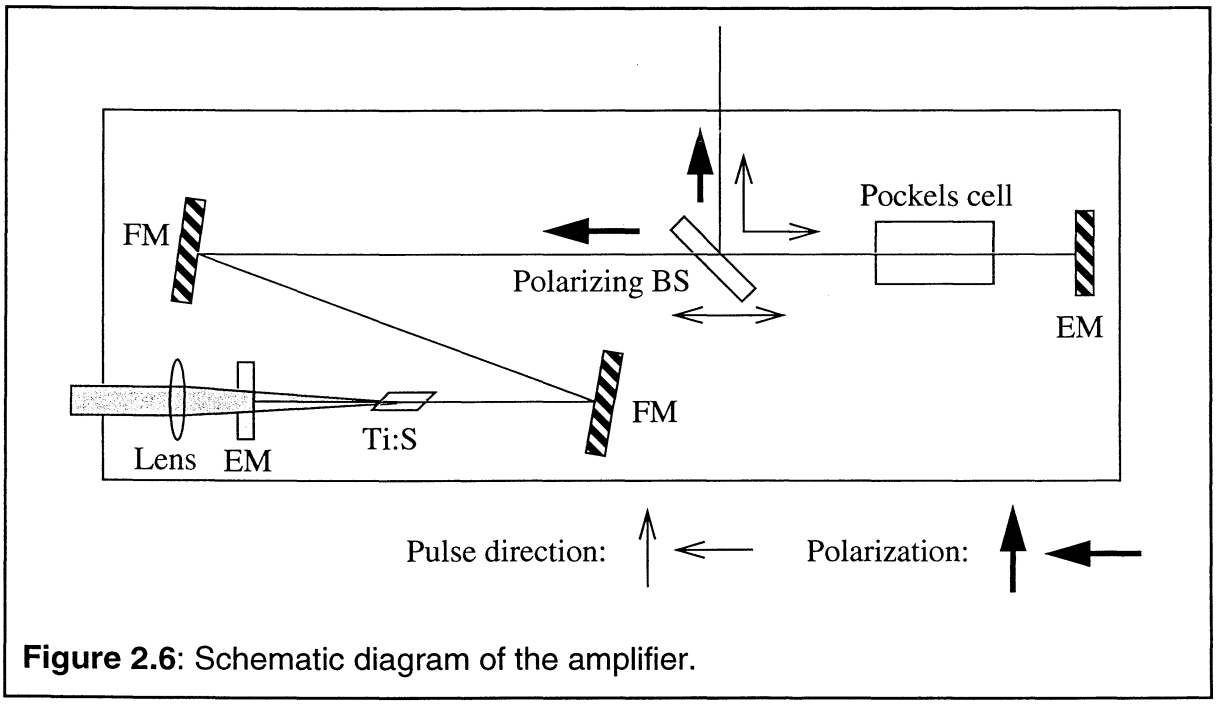

Figure 2.6: Schematic diagram of the amplifier.

The beam path through the amplifier is shown in figure 2.6. We see that the cavity is folded twice with a total resonator length of about 3 meter, which is sim-

ilar to the length of the oscillator cavity. Through a dichroic end mirror, of the cavity, the Ti:S crystal is being pumped by a Q-switched, intracavity frequency doubled Nd:YAG-laser. The pump pulses from the Nd:YAG-laser are circa 200 to 300 ns long, with a wavelength of 532 nm, an intensity of about 8-10 mJ and a repetition rate of 1 kHz. The second end mirror has got 90% reflectivity for infrared light. This for detection measurements of how the amplification is building up in the cavity. The output through this mirror can be used to monitor the pulse train in the amplifier cavity, in order to optimize the amplification of the pulse, i.e. the timing for the Pockels cell (see later).

From the stretcher, pulses with a repetition rate of 100 MHz enter the amplifier. But since the Nd:YAG-laser only pulses once every 1 kHz, only 1000 of the 10^8 pulses that enter the amplifier can be amplified every second. The KD*P crystal in the Pockels cell is so adjusted that when the Pockels cell is not activated, (when no high voltage is applied to the crystal), the polarization of the incoming pulse is turned 45° by each passage through the Pockels cell. When the pulse now reaches the polarization beamsplitter, it is thus horizontally polarized and passes through it and enters the cavity. It is there reflected by two fold mirrors and passes through the Ti:S crystal. It is then reflected back the same way by the dichroic end mirror. When the pulse comes back to the Pockels cell, its polarization is once again turned 45° by each passage, whereby it is reflected out of the cavity by the polarizing beamsplitter. The two passes through the crystal, has not at all, or only little, amplified the pulse, due to weather the crystal had an inverted population or not. This happens to most of the pulses that enter the amplifier. To be able to amplify a pulse, the Pockels cell has to be activated, so that the pulse that is in the cavity when the Ti:S crystal is maximally inverted, is kept there. The pulse is amplified by each passage through the crystal by stimulated emission into the same photon states.

The procedure described above require a synchronization of the Q-switch in the Nd:YAG-laser and the Pockels cell in the amplifier. This is accomplished by an electronic timer, which is adjusted to activate the Pockels cell when the crystal is inverted. When the Pockels cell is active, it turns the polarization of the pulse 90° by each passage through it, so that when the pulse hits the polarized beamsplitter, it now has the same polarization as it had before it passed two times through the Pockels cell. The pulse that was in the cavity, will thus keep its horizontal polarization and stay within the cavity, while a pulse coming from the stretcher is reflected out again without ever entering the cavity. The Pockels cell now stays activated for about 100 ns. The pulse that is being amplified, is kept in the cavity for the same amount of time. This is enough time for the pulse to pass ten to twelve times back and forward in the cavity, and thus pass 20 - 24 times

through the Ti:S crystal. This gives us an amplification factor of 10^5 - 10^6. In this time a TEM_{00} mode is established in the cavity. After the 100 ns, the Pockels cell is deactivated, and the polarization is then only turned 45° by each passage through it. The pulse thus changes its polarization back to vertical by two passages through the Pockels cell and is reflected out of the amplifier by the polarizing beamsplitter.

The time difference between two pulses coming from the stretcher is about 10 ns. The Pockels cell has got rise and fall times of 8 ns [CLA-95]. So if the Pockels cell is activated directly after that a pulse enters the cavity, and deactivated as the amplified pulse has just entered the cavity for its last round, not more than one pulse at a time is switched in and out without any losses. The exact time that the Pockels cell is activated is therefore manually adjustable.

As the gain of Ti:S has its maximum at 790 - 800 nm, a seed pulse with a different wavelength will experience a shift towards that peak wavelength. This is due to inhomogeneous gain for different spectral components in the amplifier cavity. For seed wavelength around 770 nm a shift of about 5 nm to the red is observed. This shift has to be compensated, if the amplified pulse wavelength has to match a given value.

The amplified pulse now leaves the amplifier in the same direction as it came in. When it comes back to the beamsplitter in the optical isolation system (BS 1 in figure 2.4) it is once again reflected to pass through the $\lambda/2$-plate and the Faraday rotator. Just as at its first passage through this setup in this direction, its polarization is not changed. The amplified pulse is thus reflected by the second beamsplitter, BS 2, prohibiting it from entering the stretcher again, and directed towards the compressor.

2.4 THE PULSE COMPRESSOR

The total group velocity dispersion, that the pulse has gathered in the stretcher and in the amplifier must now, as much as possible, be compensated. This is done by the compressor, which consists of a grating and mirror setup, similar to that of the pulse stretcher. This setup though, has a negative dispersion which recombines the chirped pulses to short once again.

The efficiency of the compressor is about 0,65, which results in a pulse energy of circa 1 mJ. The pulse is shortened to a length close to that it had after the oscillator. The output from the compressor has finally a length of circa 110 fs. This corresponds to a peak intensity of circa 10 GW. The beam profile is close to a TEM_{00} mode. In figure 2.7, the autocorrelation and the spectrum of a pulse after the compressor are shown. The bandwidth is circa 14 nm at the central wavelength of about 770 nm. This is slightly more than the bandwidth after the oscillator, compare with figure 2.3 in chapter 2.1, which indicates that most of the energy that comes from the crystal in the amplifier is added to the short pulses instead of being emitted as spontaneous emission. The time bandwidth product for the pulse after the compressor thus adds up to 0,79. But as we can see, the spectrum no longer looks like a smooth $sech^2$-profile and thus the two values for the time-bandwidth product can not be compared directly for the seed and the amplified pulse.

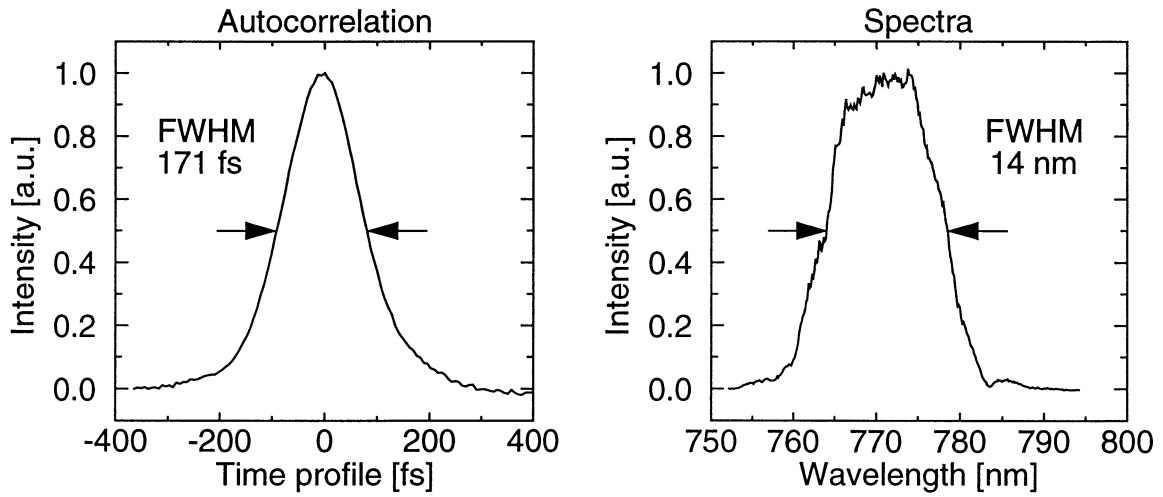

Figure 2.7: The time profile and spectra of the pulse after the compressor. The measured FWHM of the autocorrelation must be multiplied by 0,66 in order to get the correct pulse length.

3 SPECTRAL-DOMAIN SHAPING OF FEMTOSECOND LASER PULSES

3.1 SPECTRAL MODULATION SETUP

In [WEF-95], M. Wefers and K. Nelson describe an experimental setup, which performs spectral modulation of ultra short pulses. We make use of a similar setup, see figure 3.1.

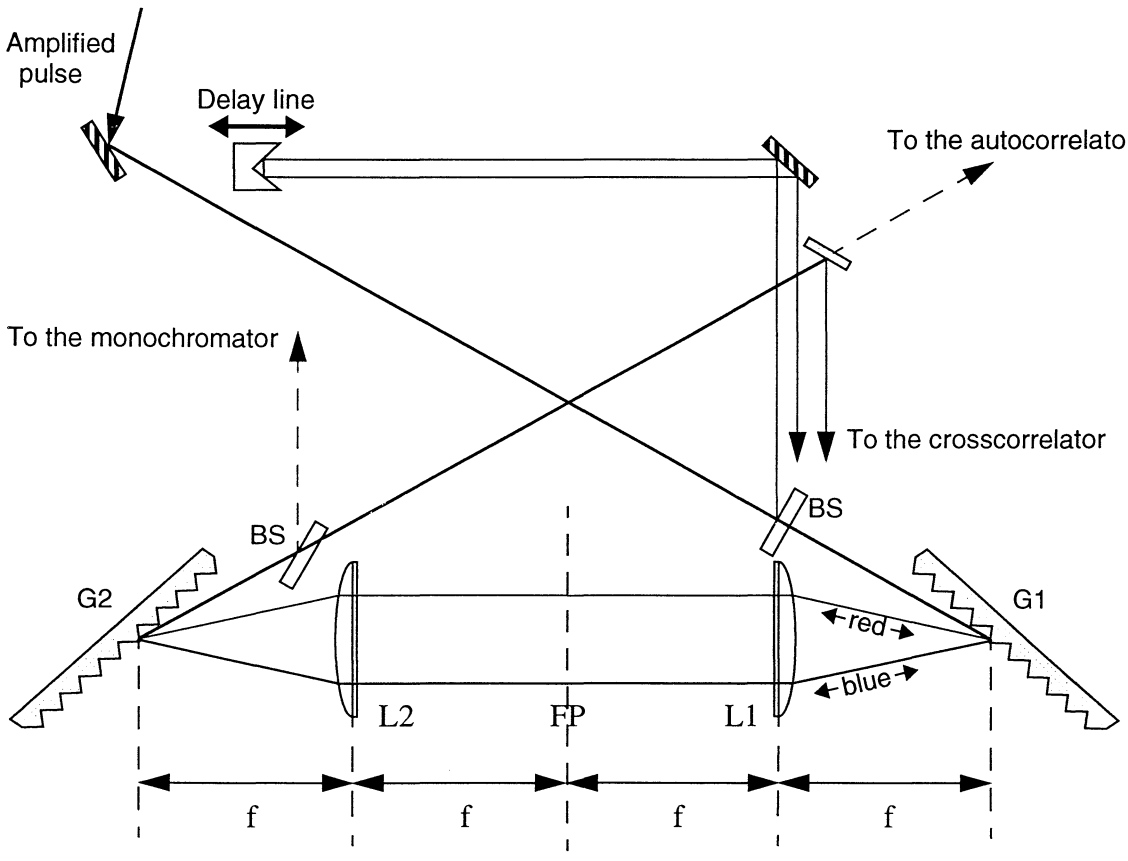

Figure 3.1: The setup for producing spectral modulations. BS: Beamsplitters, G1,2: Gratings, L1,2: cylindrical lenses, FP: Fourier plane.

Grating G1 diffracts the different frequency components of the pulse into different angular directions. The grating is placed in the backside focal plane of a plano-convex cylindrical lens, L1. The lens focuses components with the same

frequency to a common spot in its front side focal plane. Because it is a cylindrical lens, the different frequencies will be focused into vertical lines. Each frequency component is imaged to a different spatial position, which results in a well separated spectrum. Thus, this setup constitutes a transformation of the pulse from the time domain into the frequency domain. In the Fourier plane, FP, an amplitude or phase mask can be introduced. A second lens, L2, is placed so that its backside focal plane corresponds to the position of the Fourier plane, FP (con-focal arrangement of L1 and L2). The second lens collimates the spectral components and directs them toward a second grating, G2, placed in the front focal plane of L2. L2 and G2 thus recombine the spectrally modulated pulse into a collimated output beam. By adjusting the position and angles of the two lenses and gratings, (without any mask in the FP), the setup is optimized, by monitoring the beam profile, the autocorrelation (the time profile) and the spectrum of the pulse. The aim is to achieve the same parameters as for the input pulse, see figure 3.2.

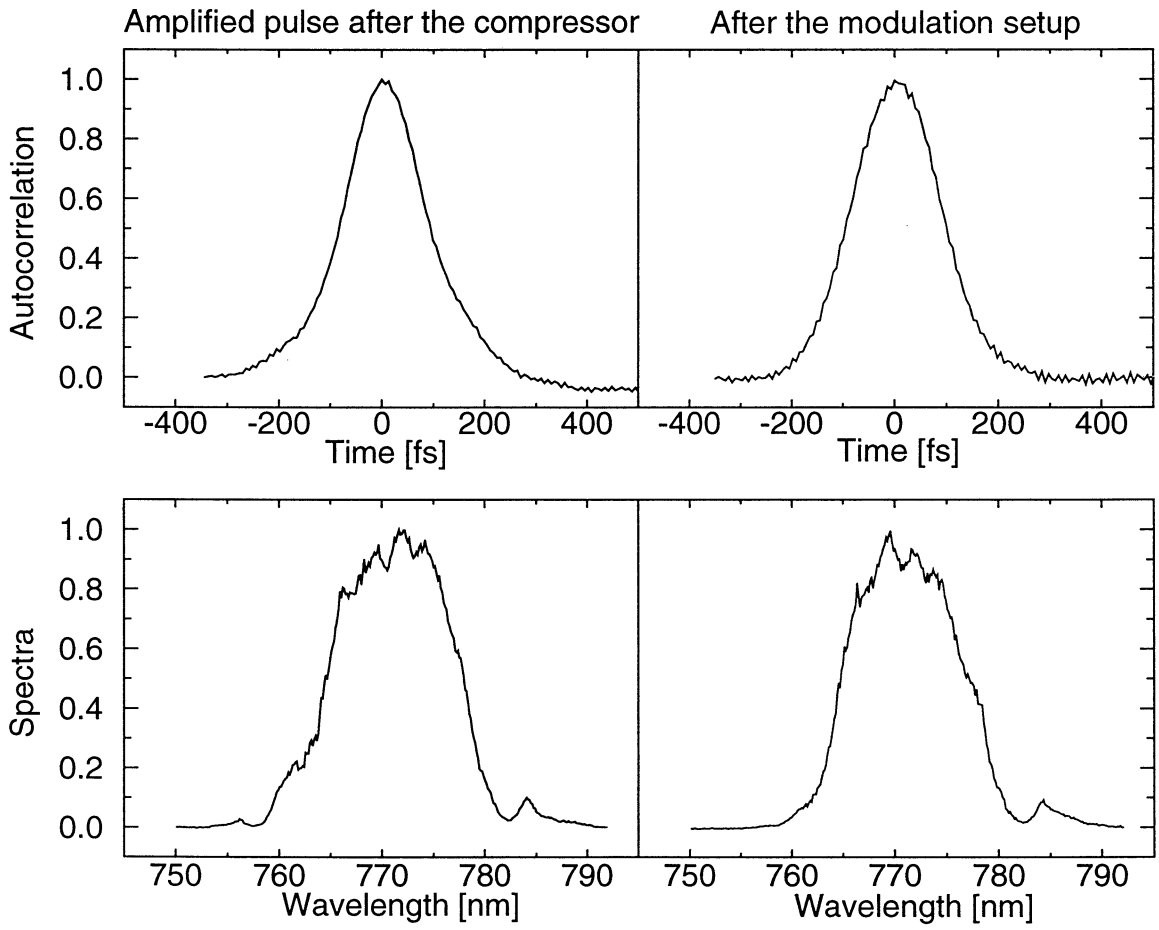

Figure 3.2: The autocorrelation and the spectra of the amplified pulse before and after the modulation setup.

Using the monochromator and a CCD camera read out by an oscilloscope, see figure 3.1, it is easy to see how the spectrum is changing in real time when an amplitude mask is introduced and moved in the Fourier plane.

The spectral resolution in the FP can easily be measured by inserting an amplitude mask of given dimensions. Using a calibrated slit with 1 mm aperture, the width of the transmitted spectrum was 2,5 nm. The same value is obtained by measuring the spectral shift of any feature of the amplitude mask (e.g. an edge) if the mask is translated transversely in the FP by 1 mm.

3.2 SPATIAL LIGHT MODULATORS (SLM)

In the FP of the modulation setup, the pulse spectrum is spatially dispersed. Any spatial amplitude or phase object can be introduced in this position in order to modulate the spectral components. Such a device can be labelled as spatial light modulator, SLM, and consist of a mechanical amplitude mask in the simplest form. Other types of modulators can be static phase retarders (glass plate arrays), mirror assemblies or birefringent components (wave plates, liquid crystal arrays).

3.2.1 MECHANICAL AMPLITUDE MASKS

The use of diapositive slides offers the possibility of varying the transmission by applying grey scales. Some losses in the "transparent" regions still have to be taken into account. If gradual attenuation of the spectral components is not required, a mechanical bar mask can be used which blocks the corresponding components totally. This type of mask was used in our experiment, see chapter 4.2.2 and 5.3.

The main drawback of using a mechanical amplitude mask is the lack of flexibility. To achieve a different modulation pattern, the whole mask has to be exchanged. The only degree of freedom consists in the transversal translation of the mask in order to modify different frequency components. On the other hand, their advantage consists in easy production and handling and in fact, that the losses for the transmitted components are very small, or even zero.

3.2.2 LIQUID CRYSTAL ARRAY (LCA)

An other type of a SLM is a liquid crystal array, LCA. The advantage of using an LCA is the flexibility of setting up different amplitude patterns by electronically addressing of individual LC cells. It also offers a very fine adjustment of the transmission of the cells (about 3200 grey levels). The pixel array can be activated within 100 ms, which yields a maximum repetition rate of about 10 Hz for any arbitrary sequence of modulation patterns.

In contrast to its flexibility there are two restrictions to be considered. Firstly, the resolution of the spatial patterns is given by the finite size of the cells. Secondly, as the amplitude modulation is obtained by a transformation of the polarization of the light, losses in the different optical elements (polarizers, LSA) occur which reduce the efficiency of the modulator.

We used an LCA made by Meadowlark Optics (Model SLM2256, Type SSP-128) for some of our experiments. It is made up of a thin nematic liquid crystal material placed in between two silica substrates. These substrates are coated with indium tin oxide, which is an optically transparent, electrically conducting material. On one of the sides of the LC, the conducting material is divided into a linear array of 128 electrodes (pixels). These pixels have a width of 100 μm and a height of 4 mm. The distance between them is 2 μm only. The width of 100 μm corresponds, in the Fourier plane of our setup, to a spectral distance of 0,25 nm. The opposite silica substrate is not patterned, and is connected to ground.

The LC consists of rodlike molecules that tend to align in an external electric field. The macroscopic orientation of the crystal leads to a birefringence which therefore depends on the applied field. By changing the voltage the LC's birefringence can thus be controlled for each pixel. Light passing through the different pixels will then experience different phase shifts, modifying its polarization from, e.g. being horizontal polarized, into an elliptic polarization By placing a vertical polarizer directly after the LCA, only the vertical components of the now elliptic polarized light is transmitted. Depending upon its amplitude, the intensity of the transmitted light through the pixels will be changed, see figure 3.3.

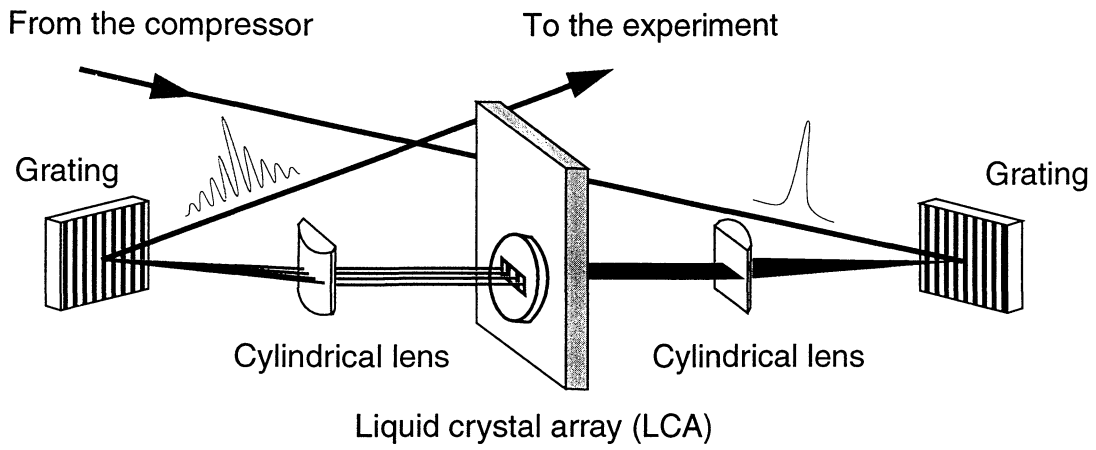

Figure 3.3: How the LCA modifies the pulse spectrum.

The transmitted intensity as a function of the voltage over the pixel, has been measured, [GAL-96]. To be able to do a correct simulation of its operation, we have to take into account how the phase of the spectral component changes, when passing through the LCA. The simulation of the resulting pulse amplitude in the time domain corresponds well to the experimental data only if this phase shift is included in the calculation. In figure 3.4, figure 3.5 and figure 3.6, some spectral modulations that were realized with the LCA, the measured crosscorrelation for these modulations, and the simulation of the corresponding time signals, are shown.

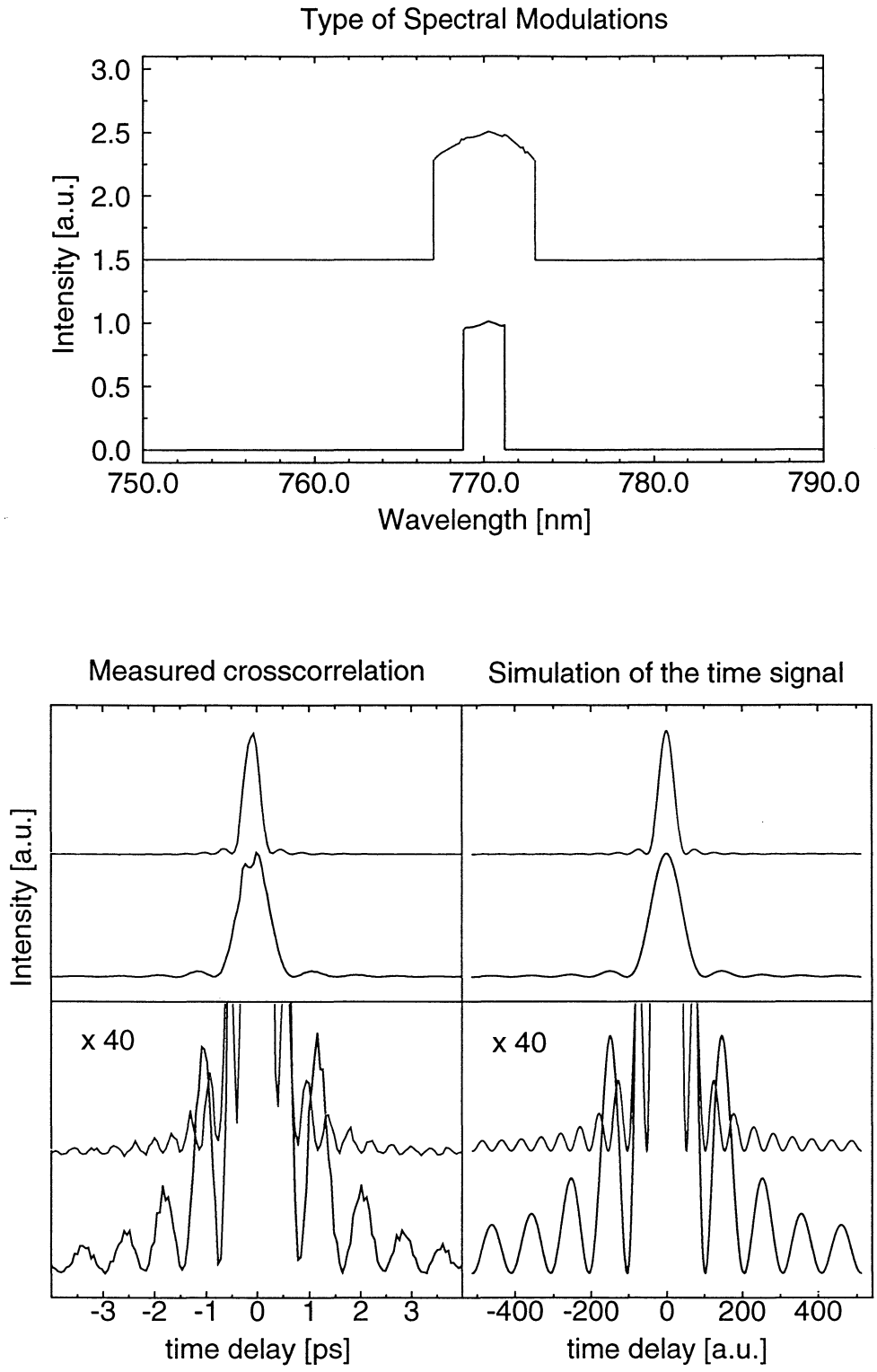

Figure 3.4: The two types of single rectangle modulations, with 5 and 10 pixels opened respectively, that were performed with the LCA, the measured time signal for these modulations, and the simulation of the time signal, correspondingly. The time signals have also been enlarged 40 times, to show how well the experimental and the simulation do correspond.

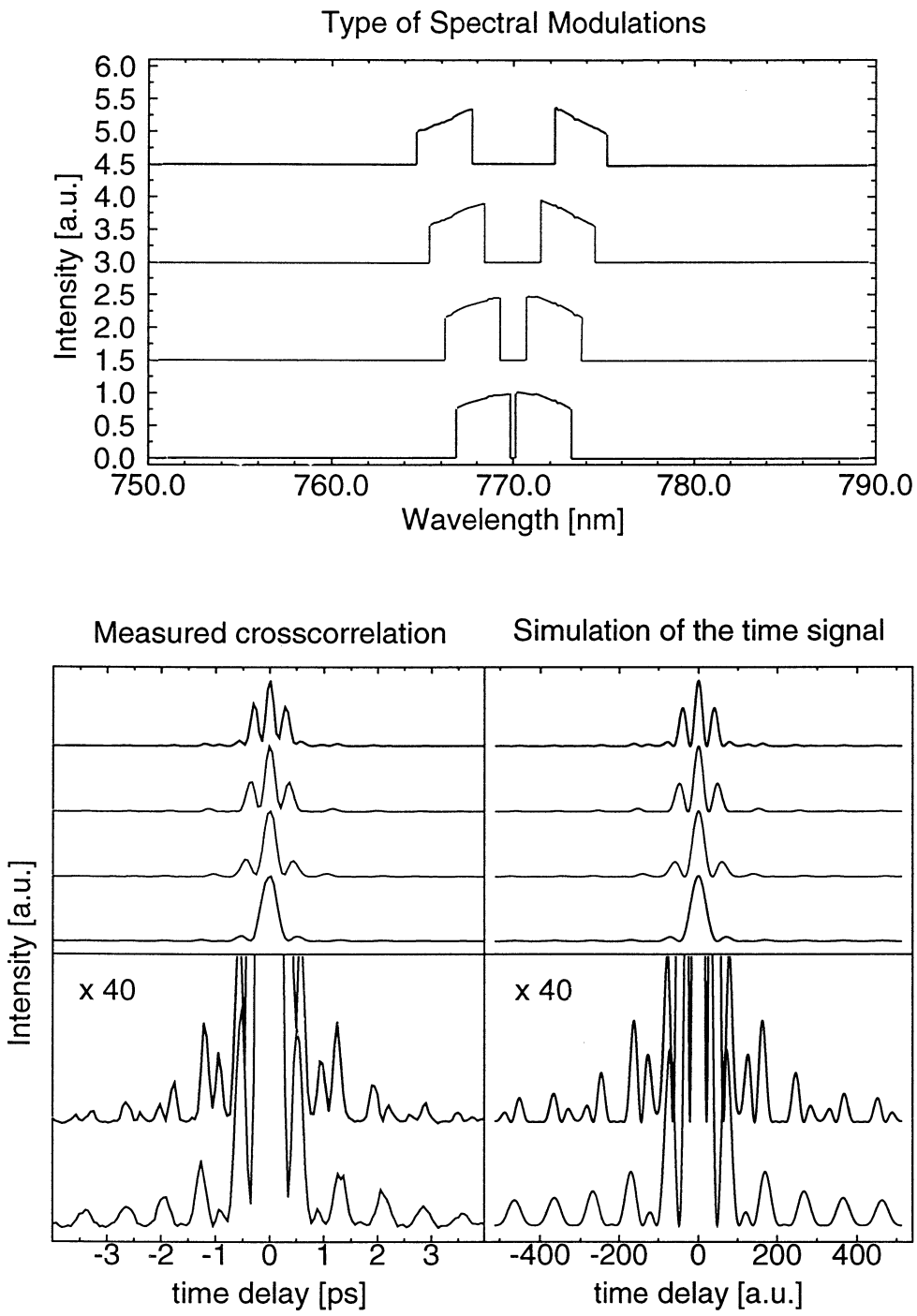

Figure 3.5: The four types of rectangle modulations with an area of 10 pixels opened and a gap of 1, 5, 10 and 20 pixels, respectively that were set up with the LCA. The measured crosscorrelation for these modulations, and the simulation of the time signal for these rectangular modulations. For the 1 and 20 pixel gaps, the time signals have also been enlarged 40 times, to show the correspondence of the experimental data with the simulation.

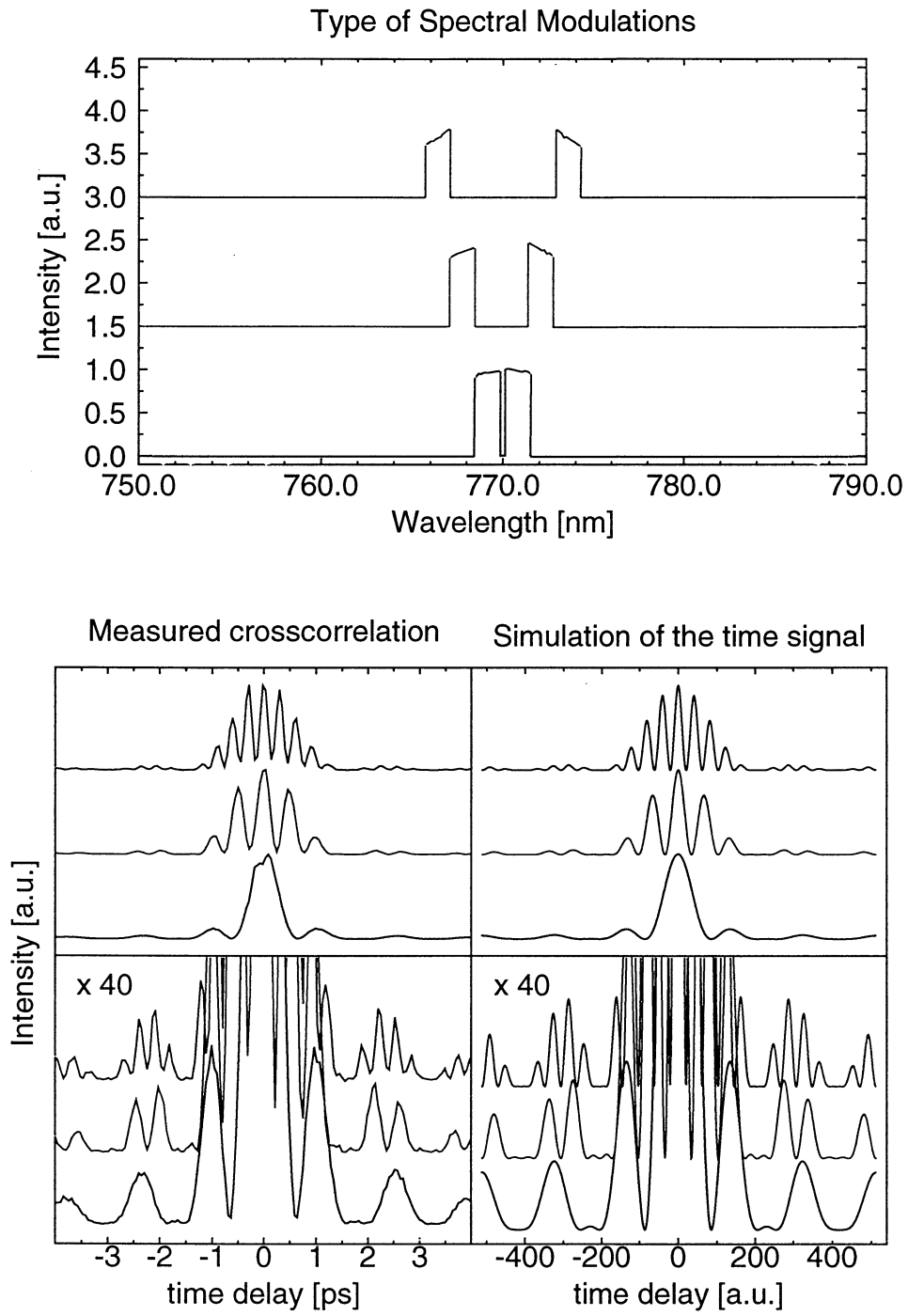

Figure 3.6: The four types of rectangle modulations with an area of 5 pixels opened and a gap of 1, 10 and 20 pixels, respectively that were performed with the LCA. The measured crosscorrelation for these modulations, and the simulation of the time signal for these rectangular modulations. The time signals have also been enlarged 40 times, to show how well the experimental data and the simulation do correspond.

4 FEMTOSECOND TWO PULSE PHOTON ECHO

4.1 THEORY

4.1.1 DENSITY MATRIX FORMALISM

It is known from quantum mechanics that we can describe the state of the atomic system by a wavefunction: $\Psi(\boldsymbol{r}, t)$. The wavefunction describes the probability of finding the state at time t at the position $\boldsymbol{r}$.

The process of measuring a physical quantity of the system (energy, momentum etc.) corresponds to operation on the state vector by the operator corresponding to the physical observable. These types of operators are called Hermitian operators and they have the characteristic that the adjoint of the operator is equal to the operator itself, $\hat{A}^{\dagger} = \hat{A}$ [YAR-89].

Let $\hat{A}$ be a Hermitian operator corresponding to some observable in the system. The effect of Hermitian operators in space, is to alter, in general, the direction and magnitude of the vectors on which they operate. The eigenvectors of a given operator, say $\hat{A}$, are those vectors whose direction in space are not altered when operated on by $\hat{A}$.

An example of a Hermitian operator is the total Hamiltonian $\hat{H}$. If $\Psi(\boldsymbol{r}, t)$ is an eigenfunction to $\hat{H}$, (this will be explained later), we get the **time dependent Schrödinger Equation, S.E.**, when letting the total Hamiltonian operate on the wavefunction $\Psi(\boldsymbol{r}, t)$:

$$\hat{H}\Psi = i\hbar\frac{d\Psi}{dt} \tag{4.1}$$

We see that letting the Hamiltonian operator operate on the wavefunction, means in fact not much more than a time derivation of the wavefunction. We can compare the calculation for obtaining the solution to the wavefunction, with any

other linear, homogenous first order differential equation in one variable, for example:

$$\frac{dN}{dt} = -\lambda N$$

We make an ansatz, consisting of a time dependent part, $e^{-\lambda t}$, and a time independent part, N_0, made up by the solution to the time independent equation:

$$N = N_0 \cdot e^{-\lambda t}$$

and try it

$$\frac{dN}{dt} = -\lambda \cdot N_0 \cdot e^{-\lambda t} = -\lambda N$$

Our ansatz was a correct one, and thus is $N = N_0 \cdot e^{-\lambda t}$ a solution to the time derivative equation. In the same way the solution for the Hamilton operator, equation (4.1), is found.

$$\hat{H}\Psi = i\hbar\frac{d\Psi}{dt}$$

Our ansatz:

$$\Psi(t) = \Psi(0) \cdot e^{-\frac{i \cdot \hat{H} \cdot t}{\hbar}} \tag{4.2}$$

consists of a time dependent part, $\exp{-(i \cdot \hat{H} \cdot t)/\hbar}$, and a time independent part, $\Psi(0)$, made up from the solution to the time independent S.E. This latter part makes up the basis function, or rather, the eigenfunction of the time-independent Hamiltonian. Inserting our ansatz in the differential equation gives:

$$i\hbar \cdot \left(-\frac{i \cdot \hat{H}}{\hbar} \cdot \Psi(0) \cdot e^{-\frac{i \cdot \hat{H} \cdot t}{\hbar}} \right) = \hat{H}\Psi$$

This means that our ansatz was correct and that equation (4.2) is a solution to the S.E.

The wave function itself can be expanded in terms of any basis function, φ_i and φ_j, which describe its position in space. If these functions are chosen in such a way that they are the eigenfunctions of an operator $\hat{A}$, ϕ_i and ϕ_j, one gets a simplified, straightforward mathematical description of how the operator affects the system.

Here we introduce the **Dirac Notation**. This is a mathematical abbreviation so to say, because it is written in the same way, but is calculated differently depending upon if the operator is operating on a function or a vector. Dirac notation for a function is written and means:

$$\langle \Psi | A | \Psi \rangle = \int \Psi^*(\boldsymbol{r},t) A \Psi(\boldsymbol{r},t) d\boldsymbol{r} \tag{4.3}$$

and for a vector:

$$\langle \Psi | A | \Psi \rangle = \begin{bmatrix} c_1^* & c_2^* \end{bmatrix} \begin{bmatrix} a_{11} & a_{12} \\ a_{21} & a_{22} \end{bmatrix} \begin{bmatrix} c_1 \\ c_2 \end{bmatrix}$$

By using Dirac Notation, we don't have to care about whether the operator is operating on a function or a vector. The formalism is the same.

In general, any arbitrary set of basis functions are not orthogonal to each other. This written with Dirac Notation is:

$$\langle \varphi_i | \varphi_j \rangle \neq \delta_{ij}$$

but for a basis of eigenfunctions, when $\hat{A}$ is taken to be Hermitian, they are:

$$\langle \phi_i | \phi_j \rangle = \delta_{ij} \tag{4.4}$$

Where δ_{ij} is the Kronecker delta which is:

$$\delta_{ij} = 0 \text{ for } i \neq j \text{ and}$$

$$\delta_{ij} = 1 \text{ for } i = j$$

What also is true for any basis function in general, is that a_i is not an eigenfunction to $\hat{A}$:

$$\hat{A}|\varphi_i\rangle \neq a_i|\varphi_i\rangle$$

while for a basis of eigenfunctions, it is:

$$\hat{A}|\phi_i\rangle = a_i|\phi_i\rangle \tag{4.5}$$

To see how the operator affects the wavefunction, we, for now, postulate that all we need to calculate are the different matrix elements in the matrix: $A_{ij} = [\langle\phi_i|\hat{A}|\phi_j\rangle]_{ij}$. That this is true will bee shown from equation (4.8). The calculation of the different matrix elements is done in the following way for functions [YAR-89]:

$$A_{ij} = \int(\phi_i^* \cdot \hat{A} \cdot \phi_j) \tag{4.6}$$

Using (4.5) in (4.6) yields:

$$A_{ij} = a_j\int(\phi_i^* \cdot \phi_j)dx$$

And after making use of (4.4), the equation has been reduced to

$$A_{ij} = a_j \cdot \langle\phi_i|\phi_j\rangle$$

Which gives us a diagonal matrix:

$$[\langle\phi_i|\hat{A}|\phi_j\rangle]_{ij} = \begin{bmatrix} a_i & 0 \\ 0 & a_j \end{bmatrix} \tag{4.7}$$

Considering this short and schematic survey of what happens, one can conclude that it is smart to choose to expand the wavefunction in terms of the eigenfunctions, u_n, of the operator $\hat{A}$, that is:

$$\Psi(\boldsymbol{r},t) = \sum c_n(t)u_n(\boldsymbol{r}) \tag{4.8}$$

All the spatial information lies now in the different $u_n's$, while the temporal information is found in the $c_n's$. The spatial information depends on the exact nature of the state, e.g., as described by its quantum numbers: S, P, D, F, etc.

As assumed above, the $u_n's$ are eigenstates of $\hat{A}$:

$$\hat{A}|u_n\rangle = a_n|u_n\rangle \tag{4.9}$$

The eigenvalues, a_n, constitute the set of all possible measurements of the observable A. The probability that any given value, a_n, is found by the measurement at time t is $|c_n(t)|^2$, where:

$$c_n(t) = \int u_n^*(\boldsymbol{r}) \cdot \Psi(\boldsymbol{r},t)d\boldsymbol{r} \tag{4.10}$$

According to this interpretation, the expectation value of $\hat{A}$ is:

$$\langle A(t)\rangle = \sum_n a_n|c_n(t)|^2$$

which leads to:

$$\langle A(t)\rangle = \sum_n a_n \int(\Psi^*(\boldsymbol{r},t) \cdot u_n(\boldsymbol{r}))d\boldsymbol{r} \int(\Psi(\boldsymbol{r}',t) \cdot u_n^*(\boldsymbol{r}'))d\boldsymbol{r}'$$

Using (4.9) we get:

$$\langle A(t)\rangle = \int(\Psi^*(\boldsymbol{r},t) \cdot A)\left(\int \Psi(\boldsymbol{r}',t)\sum_n u_n^*(\boldsymbol{r}') \cdot u_n(\boldsymbol{r})d\boldsymbol{r}'\right)d\boldsymbol{r} \tag{4.11}$$

The summation in the end of the equation above is equal to the Dirac delta, compare with (4.4) This turns the second integral in the equation above into:

$$\int(\Psi(\boldsymbol{r}',t) \cdot \delta(\boldsymbol{r}-\boldsymbol{r}'))d\boldsymbol{r}' = \Psi(\boldsymbol{r},t)$$

giving that (4.11) results in:

$$\langle A(t)\rangle = \int \Psi^*(\boldsymbol{r},t) A \Psi(\boldsymbol{r},t) d\boldsymbol{r} \tag{4.12}$$

The equation (4.12) can be rewritten in Dirac Notation, see equation (4.3), as:

$$\langle A\rangle = \langle \Psi(\boldsymbol{r},t)|A|\Psi(\boldsymbol{r},t)\rangle$$

which was postulated before, see equation (4.6).

Insertion of (4.8) gives us:

$$\langle A\rangle = \sum_{n,\,m} c_m^*(t)\langle u_m(\boldsymbol{r})|A u_n(\boldsymbol{r})\rangle c_n(t)$$

By making use of (4.6), we obtain:

$$\langle A\rangle = \sum_{n,\,m} c_m^* A_{mn} c_n = \sum_{n,\,m} c_m^* c_n A_{mn} \tag{4.13}$$

Now suppose that the precise state of the system is unknown, or that we have to describe an ensemble of quantum mechanical systems. This lack of knowledge is reflected in an uncertainty in the values of the $c_n's$ in equation (4.8). We assume, however, that we have enough information to calculate an ensemble average for $c_m^* c_n$. The average will be denoted by a bar over the quantity in question. Thus one can compute an average value over the expectation value of $\hat{A}$ according to:

$$\langle \bar{A}\rangle = \sum_{n,\,m} \overline{c_m^* c_n} A_{mn} \tag{4.14}$$

See [BOY-92] and [YAR-89]. By convenient reasons, ρ_{nm} is defined as:

$$\rho_{nm} = \overline{c_m^* c_n} \tag{4.15}$$

The matrix formed by the values of ρ_{nm} is known as the **density matrix**. By using the definition of product of matrices:

$$(AB)_{kl} = \sum_m A_{km} B_{ml}$$

We obtain:

$$\langle \bar{A} \rangle = \sum_n (\rho A)_{nn}$$

This computation is indicated by the trace, abbreviated "tr.". Thus,

$$\langle \bar{A} \rangle = tr(\rho A) \tag{4.16}$$

It follows from its definition that $\rho_{mn} = \rho_{nm}^*$.

In the physical interpretation, the density matrix represents certain probabilistic aspects of the ensemble. Notice that the elements on the diagonal of the density matrix, ρ_{nn}, are real numbers which correspond to the probability of being in the different states. The sum of the diagonal elements should be one, which follows from the normalization criterion of the wavefunction $\Psi(\boldsymbol{r},t)$. Thus:

$$tr\rho = \sum_m \overline{c_m^* c_m} = 1 \tag{4.17}$$

The off-diagonal elements, ρ_{nm}, on the other hand, are complex numbers whose meaning is related to the phase of transitions between m and n. They give the "coherence" between the levels n and m, in the sense that ρ_{nm} describes the transition between the states. This means a coherent superposition of the two eigenstates n and m.

But the density matrix does not give us information about how the system is changing in time. For this we need the time evolution of the density matrix. From the definition of the density matrix, (4.15), we get:

$$\frac{\partial \rho_{nm}}{\partial t} = c_n \cdot \frac{\partial}{\partial t} c_m^* + c_m^* \cdot \frac{\partial c_n}{\partial t} \tag{4.18}$$

Now what does this mean? For this we need to develop the Schrödinger equation, (S.E.). Since the wavefunction of every systems in the ensemble satisfies the S.E., then:

$$\hat{H}\Psi = i\hbar\frac{\partial}{\partial t}\Psi(\boldsymbol{r},t)$$

is true for the whole ensemble. By substituting the expanded wavefunction (4.8) for $\Psi(\boldsymbol{r},t)$, we get:

$$i\hbar\sum_n\frac{\partial}{\partial t}c_n(t)u_n(\boldsymbol{r}) = \sum_n c_n(t)\hat{H}u_n(\boldsymbol{r})$$

which is reduced to the equation

$$i\hbar\frac{\partial}{\partial t}c_m(t) = \sum_n c_n(t)H_{mn}$$

by taking the inner product of the last equation with $u_m(r)$ and using the orthonormality of the $u_n's$. Alteration gives:

$$\frac{\partial}{\partial t}c_m(t) = \frac{-i}{\hbar}\sum_n c_n(t)H_{mn} \tag{4.19}$$

To easily compare (4.19) with (4.18) we change the index of the equation (4.19) into:

$$\frac{\partial c_n}{\partial t} = \frac{-i}{\hbar}\sum_k c_k H_{nk} \tag{4.20}$$

and

$$\frac{\partial}{\partial t}c_m{}^* = \left(\frac{\partial c_m}{\partial t}\right)^* = \left(\frac{-i}{\hbar}\sum_k c_k H_{mk}\right)^* = \frac{i}{\hbar}\sum_k c_k{}^* H_{mk}{}^* = \frac{i}{\hbar}\sum_k c_k{}^* H_{km} \tag{4.21}$$

The last step follows from the fact that the Hamiltonian is a Hermitian operator. By combining the equations, (4.20), (4.21) and (4.18), we get:

$$\frac{\partial \rho_{nm}}{\partial t} = \frac{-i}{\hbar}\sum_k c_n c_k^* H_{km} - \frac{i}{\hbar}\sum_k H_{nk} c_k c_m^*$$

Because of the definition of ρ_{nm}, equation (4.15), we get:

$$\frac{\partial \rho_{nm}}{\partial t} = \frac{i}{\hbar}\left(\sum_k \rho_{nk} H_{km} - \sum_k H_{nk}\rho_{km}\right) = \frac{i}{\hbar}[\rho_n H_m - H_n \rho_m] = \frac{i}{\hbar}[\hat{\rho},\hat{H}] \quad (4.22)$$

This time dependent Schrödinger equation is called the **Liouville-von Neumann equation**.

The two-level approximation

Now we choose to introduce the assumption that only two levels, let us say the ground and an excited state of a dye molecule, are involved in the interaction. These two levels: level a and level b, have got two different energies: E_a and E_b, as shown in figure 4.1. A transition between two levels in an atom or in a molecule occur when the atom/molecule absorb a photon with an energy equal to the energy difference between the two levels, from an external electrical field. Thus is the assumption that only two levels are involved in the interaction justified only when the angular frequency ω of the field has got the suitable energy for the transition only between level a and level b. The external fields frequency must thus satisfy $\omega \sim \omega_{ba} = (E_b - E_a)/\hbar$. As a result, the density matrix is reduced to a 2×2 matrix with the elements ρ_{aa}, ρ_{ab}, ρ_{ba} and ρ_{bb}.

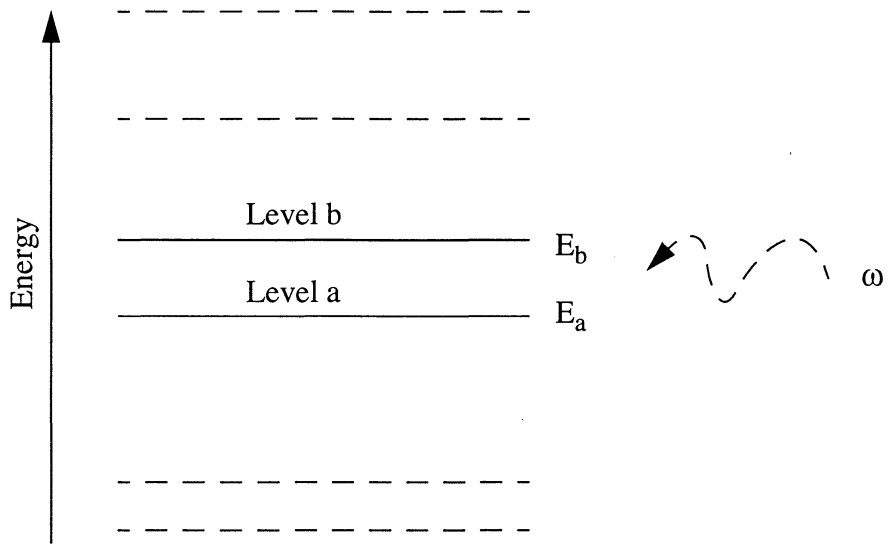

Figure 4.1: A two-level system interacting with a radiation field whose frequency ω fulfils: $\omega \sim \omega_{ba} = (E_b - E_a)/\hbar$. Other levels that are nonresonant (shown here by broken lines) are assumed to play no role in the interaction.

When the unperturbed Hamiltonian $\hat{H}_o$ operates on its eigenfunctions, the eigenvalues corresponds to the energy of the states. The matrix representation of $\hat{H}_o$ is diagonal in the basis of its eigenfunctions, that is: $H_{0,nm} = E_n \cdot \delta_{nm}$, compare with equation (4.7).

$$[\langle \phi_i | \hat{H}_o | \phi_j \rangle]_{ij} = \begin{bmatrix} E_a & 0 \\ 0 & E_b \end{bmatrix}$$

The unperturbed Hamiltonian, $\hat{H}_o$, describes the stationary state of the system, but it can't describe the effect of an external field. This is described by an other time dependent Hamiltonian, $V(t)$. The external forces on the system must be known in order to derive the interaction Hamiltonian. The external force is: $\boldsymbol{F} = e \cdot \boldsymbol{E}(\boldsymbol{r},t)$, where e is the charge of the electron, $\boldsymbol{r}$ is the position vector in the three dimensional space, and $\boldsymbol{E}$ is the electric field. The electric field is:

$$\boldsymbol{E}(\boldsymbol{r},t) = \boldsymbol{E_0}\cos(\omega t) \tag{4.23}$$

Using $\boldsymbol{F} = -\nabla V$ and that the electric dipole moment is $\mu = -e\boldsymbol{r}$, the external potential can be expressed as:

$$V = -\mu \cdot \boldsymbol{E}(\boldsymbol{r},t) \tag{4.24}$$

This potential is the interacting Hamiltonian, where μ is the component of the dipole operator along the direction of the field $\boldsymbol{E}(\boldsymbol{r},t)$. The total Hamiltonian is thus the sum of the unperturbed Hamiltonian and the interaction Hamiltonian:

$$H(t) = H_0 + V(t) \tag{4.25}$$

The diagonal matrix elements of V are taken as zero

$$\mu_{aa} = \mu_{bb} = 0 \tag{4.26}$$

so that the matrix description of the interacting Hamiltonian is the following:

$$V(t) = \begin{bmatrix} 0 & V_{ab}(t) \\ V_{ba}(t) & 0 \end{bmatrix}$$

This, equation (4.26), is true for atoms and for molecules, without permanent dipole moment. For these types of systems, this can be shown by including the phase in the wavefunction:

$$\mu_{aa} = \int \Psi_a^* (e^{-i\varphi_a t})^* \hat{\mu} \Psi_a (e^{-i\varphi_a t}) d\boldsymbol{r}$$

When the states have got definite parity, we are allowed to write the equation as,

$$\mu_{aa} = \int \mu \Psi_a^* \Psi_a dx = 0$$

because the integral over an odd function is always zero. The same argument follows for μ_{bb}. For the off diagonal elements, the same argument need not be true. If the two wavefunctions have got different parity, then the integral:

$$\mu_{ab} = \int \Psi_a^* (e^{-i\varphi_a t})^* \hat{\mu} \Psi_b (e^{-i\varphi_b t}) dx \neq 0$$

If the phases φ_a and φ_b are, without loss of generality, taken to be equal, then

$$\mu_{ab} = \mu_{ba} = \mu \tag{4.27}$$

By calculating the ensemble average $\langle\mu\rangle$, we'll get information about how the molecules interact with a field $\boldsymbol{E}(\boldsymbol{r},t)$. The value of $\langle\mu\rangle$ is given according to (4.16) by

$$\langle\mu\rangle = tr(\rho\mu) = \rho_{ab}\mu_{ba} + \rho_{ba}\mu_{ab} + \rho_{aa}\mu_{aa} + \rho_{bb}\mu_{bb}$$

Using (4.26) and (4.27), we get:

$$\langle\mu\rangle = \mu(\rho_{ab} + \rho_{ba})$$

As we can see the induced electric dipole moment is proportional to the off-diagonal elements of the density matrix.

We can now calculate how the different density matrix elements change in time, by inserting the total Hamiltonian, equation (4.25) in the Liouville-von Neumann equation (4.22).

$$\frac{d\rho_{ba}}{dt} = \frac{i}{\hbar}\left(\sum_k \rho_{bk}H_{ka} - \sum_k H_{bk}\rho_{ka}\right) =$$

$$= \frac{i}{\hbar}(\rho_{ba}\cdot H_{aa} + \rho_{bb}\cdot H_{ba}) - \frac{i}{\hbar}(H_{ba}\cdot\rho_{aa} + H_{bb}\cdot\rho_{ba}) =$$

$$= \frac{i}{\hbar}(\rho_{ba}\cdot E_a + \rho_{bb}\cdot V_{ba}) - \frac{i}{\hbar}(V_{ba}\cdot\rho_{aa} + E_b\cdot\rho_{ba}) =$$

$$= \frac{i}{\hbar}[(E_a - E_b)\rho_{ba} + V_{ba}(\rho_{bb} - \rho_{aa})]$$

The time derivation of the three other density matrix elements is calculated in a similar way, and the four equations read [MUK-95]:

$$\frac{d\rho_{aa}}{dt} = -\frac{i}{\hbar}(V_{ab}\rho_{ba} - V_{ba}\rho_{ab}) \tag{4.28}$$

$$\frac{d\rho_{bb}}{dt} = -\frac{i}{\hbar}(V_{ba}\rho_{ab} - V_{ab}\rho_{ba}) \tag{4.29}$$

$$\frac{d\rho_{ab}}{dt} = -\frac{i}{\hbar}(E_a - E_b)\rho_{ab} - \frac{i}{\hbar}V_{ab}(\rho_{bb} - \rho_{aa}) \tag{4.30}$$

$$\frac{d\rho_{ba}}{dt} = -\frac{i}{\hbar}(E_b - E_a)\rho_{ba} - \frac{i}{\hbar}V_{ba}(\rho_{aa} - \rho_{bb}) \tag{4.31}$$

We see that the solutions to our equations (4.30) and (4.31) would contain a time varying factor of the type: $\exp\pm i\omega_{ab}t$ (compare with equation (4.2)). What we want is a time-independent, or at least slowly varying solution when the frequency of the perturbing field is close or equal to the transition frequency $\omega \sim \omega_{ba} = (E_b - E_a)/\hbar$. A smart way of accomplishing that is to multiply the off-diagonal elements in our time-depending equations (4.30) and (4.31) with the complex conjugate of their time depending factor, but substituting the field frequency ω for the resonant frequency ω_{ba}. Our new density matrix elements are defined:

$$\tilde{\rho}_{ab} \equiv e^{-i\omega t} \cdot \rho_{ab}(t) \tag{4.32}$$

$$\tilde{\rho}_{ba} \equiv e^{i\omega t} \cdot \rho_{ba}(t) \tag{4.33}$$

Let us now compute the time derivative of our new density matrix elements, (4.32) and (4.33).

$$\frac{d\tilde{\rho}_{ab}}{dt} = -i\omega \cdot e^{-i\omega t} \cdot \rho_{ab}(t) + e^{-i\omega t} \cdot \frac{d\rho_{ab}}{dt}(t)$$

Insertion of (4.32) and (4.30), and the resonance frequency into this relation gives us

$$\frac{d\tilde{\rho}_{ab}}{dt} = -i\omega \cdot \tilde{\rho}_{ab} + e^{-i\omega t}\left(-i\omega_{ab} \cdot \rho_{ab} - \frac{i}{\hbar}V_{ab}(\rho_{bb} - \rho_{aa})\right)$$

By introducing the Rabi frequency Ω

$$\Omega = \frac{V_{ab}}{\hbar} = \frac{V_{ba}}{\hbar} = \frac{-\mu \cdot \boldsymbol{E}(\boldsymbol{r},t)}{\hbar}$$

and the fact that $\omega_{ab} = -\omega_{ba}$, we reduce the equation to

$$\frac{d\tilde{\rho}_{ab}}{dt} = -i(\omega - \omega_{ba}) \cdot \tilde{\rho}_{ab} - ie^{-i\omega t} \cdot \Omega \cdot (\rho_{bb} - \rho_{aa})$$

Since the electric field is oscillating harmonically with frequency ω according to equation (4.23), the Rabi frequency can be written as a cosine frequency:

$$\Omega(t) = \frac{1}{2} \cdot |\Omega| \cdot (e^{i\omega t} + e^{-i\omega t})$$

and by defining

$$\tilde{\Omega}(t) = \Omega \cdot e^{-i\omega t} = \frac{1}{2} \cdot |\Omega| \cdot (1 + e^{-2i\omega t}) \tag{4.34}$$

and the frequency detuning as

$$\Delta = \omega - \omega_{ba}$$

our equation is reduced to:

$$\frac{d\tilde{\rho}_{ab}}{dt} = -i\Delta \cdot \tilde{\rho}_{ab} - i\tilde{\Omega}(\rho_{bb} - \rho_{aa})$$

The same transformation is easily done for $d/dt\ \tilde{\rho}_{ba}(t)$ and it is also necessary to rewrite $d/dt(\rho_{aa}(t))$ and $d/dt(\rho_{bb}(t))$, since these equations also contain ρ_{ab} and ρ_{ba}. As planed $\tilde{\rho}_{ab}$ and $\tilde{\rho}_{ba}$ are slowly varying for a near resonant field.

The Liouville-von Neumann equation can now be rewritten in a matrix form as the following:

$$\frac{d}{dt}\begin{bmatrix}\tilde{\rho}_{ab}\\ \tilde{\rho}_{ba}\\ \tilde{\rho}_{aa}\\ \tilde{\rho}_{bb}\end{bmatrix} = -i\begin{bmatrix}\Delta & 0 & -\tilde{\Omega}(t) & \tilde{\Omega}(t)\\ 0 & -\Delta & \tilde{\Omega}^*(t) & -\tilde{\Omega}^*(t)\\ -\tilde{\Omega}^*(t) & \tilde{\Omega}(t) & 0 & 0\\ \tilde{\Omega}^*(t) & -\tilde{\Omega}(t) & 0 & 0\end{bmatrix}\begin{bmatrix}\tilde{\rho}_{ab}\\ \tilde{\rho}_{ba}\\ \tilde{\rho}_{aa}\\ \tilde{\rho}_{bb}\end{bmatrix} \tag{4.35}$$

$\tilde{\Omega}(t)$, see equation (4.34), contains a time-independent term and a term oscillating on twice the field frequency, 2ω. The effect of the later term is expected to be small since it oscillates much faster than any other frequency in the system. We thus neglect the time-dependent part. This approximation is called the rotating wave approximation (RWA), and write $\tilde{\Omega}(t) \cong \Omega$, [MUK-95]. The resulting Liouville-von Neumann equation can now be recast in the form

$$\frac{d}{dt}\tilde{\rho} = -\frac{i}{\hbar}[\hat{H}_{eff},\tilde{\rho}]$$

where we have introduced the effective Hamiltonian

$$\hat{H}_{eff} = \begin{bmatrix}\hbar\Delta & \hbar\Omega\\ \hbar\Omega & 0\end{bmatrix}$$

The big advantage with the effective Hamiltonian is that it is time independent. It is thus easy to let it operate on the density matrix, that is still time dependent.

Since $\rho_{aa} + \rho_{bb} = 1$ (conservation of probability, see equation (4.17)), we can eliminate one population variable and use three instead of four elements of the density operator. We further separate $\tilde{\rho}_{ab}$ into its real and imaginary parts and define:

$$u \equiv \tilde{\rho}_{ab} + \tilde{\rho}_{ba}$$

$$v \equiv i(\tilde{\rho}_{ab} - \tilde{\rho}_{ba})$$

$$w \equiv \tilde{\rho}_{aa} - \tilde{\rho}_{bb}$$

Notice that u, v and w are real. w represents the population difference and u and v are the real and imaginary parts of the off-diagonal elements in the density matrix, and thus represents the real and imaginary parts of the optical coherence.

The time behaviour of the variables u, v and w is given by that of $\tilde{\rho}$, which is a solution to the Liouville-von Neumann equation. In this model, no relaxation is introduced so far. Now we introduce relaxation by two phenomenological constants, T_1 and T_2. The relaxation effects are due to interactions between the members of the ensemble.

The relaxation times are the following:

T_1 describes the energy lifetime of the ensemble in the excited state.

T_2, describes how fast the coherence is lost. This relaxation happens due to phonons in the molecule. T_2 is called the irreversible loss off coherence time.

T_2' is a combination of the two relaxation times above according to:

$$\frac{1}{T_2'} = \frac{1}{2T_1} + \frac{1}{T_2}$$

see [MUK-95]. This relaxation time is called the coherence decay rate.

By differentiating u, using the equations implied by (4.35), and concluding from the rotating wave approximation, that $\Omega = \tilde{\Omega} = \tilde{\Omega}^*$, we see that the derivation can be rewritten in terms of v as

$$\frac{du}{dt} = \left(\frac{d\tilde{\rho}_{ab}}{dt} + \frac{d\tilde{\rho}_{ba}}{dt}\right) =$$

$$= -i(\Delta\tilde{\rho}_{ab} - \Omega\tilde{\rho}_{aa} + \Omega\tilde{\rho}_{bb}) - i(-\Delta\tilde{\rho}_{ba} - \Omega^*\tilde{\rho}_{bb} + \Omega^*\tilde{\rho}_{aa}) =$$

$$= -i\Delta(\tilde{\rho}_{ab} - \tilde{\rho}_{ba}) + i(\tilde{\rho}_{bb} - \tilde{\rho}_{aa})(\Omega - \Omega) = -\Delta v$$

By doing so for u and w too, and by introducing the relaxation using the definitions:

$$\Gamma_1 = \frac{1}{T_1}$$

and

$$\Gamma_2' = \frac{1}{T_2'}$$

we can finally write the **Bloch equations**:

$$\dot{u} = -\Delta v - \Gamma_2' u \tag{4.36}$$

$$\dot{v} = \Delta u - 2\Omega w - \Gamma_2' v \tag{4.37}$$

$$\dot{w} = 2\Omega v - \Gamma_1 (w - w_0) \tag{4.38}$$

where w_0 means the initial population. Since all the coefficients are time independent, we can obtain a general solution for any arbitrary field strength. Because of the relaxations included in the Bloch equations, the nature of the time evolution changes dramatically and the system reaches a steady state very quickly, which is obtained by setting $\dot{u} = \dot{v} = \dot{w} = 0$. But by prolonging the lifetime of our system by, as in our experiment, cooling the sample to 2,3 K, we can get some other types of results, as photon echoes, which we can understand by solving the Bloch equations. To make it easier to survey, the three Bloch equations are described as the three components of a vector, which's movement can be described in a cartesian coordinate system, see chapter 4.1.2.

4.1.2 BLOCH VECTOR FORMALISM

To make the Bloch equations more easy to survey, the Bloch equations are described in a three dimensional graph, where the different axis are made up by the three variables, u, v and w, [KRÖ-96]. This three dimensional graph will be called the **Bloch diagram**. The **Bloch vector, R**, pointing out from the origin in the Bloch diagram is defined as:

$$\boldsymbol{R} = (u,v,w)$$

The length of the Bloch vector is thus,

$$|\boldsymbol{R}| = \sqrt{(u^2 + v^2 + w^2)} = 1$$

which we get from taking the time derivative of the three Bloch equations, (4.36), (4.37) and (4.38), neglecting the relaxation processes and the knowledge that at time $t = 0$, the whole population is in the ground level. The Bloch vector is thus, when the relaxation processes are neglected, a vector pointing out from the origin at some coordinate in the (u, v, w)-space with a length of unity, see figure 4.2.

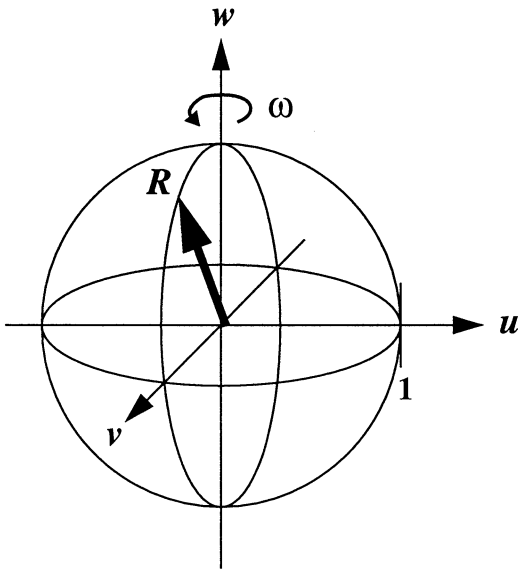

Figure 4.2: The Bloch vector, $\boldsymbol{R}$, pointing out with the length one in the space made up by the three coordinates u, v and w.

The whole Bloch diagram is rotating around the w-axis at the field frequency ω, see equation (4.34), where the RWA is introduced. In our case, when the excitation pulse consists of many different frequencies, the Bloch diagram is chosen to rotate around the w-axis at the central field frequency.

When the whole population is in the ground level, the arrow points to $w = -1$. This, since we then don't have any off-diagonal elements in the density matrix, and thus no coherence between the two levels.

How do the relaxation processes alter the direction and length of the Bloch vector? The factor Γ_1 relaxes the component in the w-direction towards the value $w = w_0 = -1$. The factor Γ_2' strives to let $u \to 0$ and $v \to 0$. The latter leads to a decrease of the length of the Bloch vector.

Let us now examine the Bloch equations: (4.36), (4.37) and (4.38). How is the Bloch vector changed by an external field, and what happens after the field is turned off?

When the system is effected by a field (characterized by $\Omega \neq 0$ and $\Omega \gg \Delta, \Gamma_1, \Gamma_2$) the Bloch vector starts to move away from $R = (0, 0, -1)$. If the detuning factor, Δ, is equal to zero, we see from the three Bloch equations, (4.36), (4.37) and (4.38), that the Bloch vector will move only in the (v, w)-plane. We define the pulse area of an excitation pulse to be the number of degrees it forces the Bloch vector to turn around the u-axis.

If $\Delta \neq 0$, the Bloch vector will also be influenced by equation (4.36) and rotate around the w-axis, which can be seen in figure 4.3. Here a simulation of the movement of the Bloch vector in time is shown, when the detuning, Δ, is set to 58,9 cm^{-1}. The trace of the vector tip in time is drawn in the upper figure to the left, a). The thicker line-width in the beginning marks the movement of the Bloch vector during the excitation (FWHM = 100 fs of the excitation pulse). Figure c) shows the Bloch diagram from a top view. Figure b) shows the Bloch vector's coordinates in the three different direction, red for u, green for v and black for w, and finally, d) shows how the absolute length of the Bloch vector is changing in time.

When the excitation is turned off, the Bloch vector, which now is pointing in a certain direction, starts to move according to the Bloch equations, with $\Omega = 0$. So, as time goes by, and if no further perturbation (field interaction) of the system occurs, e.g. a second pulse, the coherence decay rate, Γ_2', describes the movement towards the w-axis, and the inverse lifetime, Γ_1, that the Bloch vector strives towards the point $\boldsymbol{R} = (0,0,-1)$. We see the influences of the relaxation on the Bloch vector by observing the trace of the vector tip after the thicker line-width in figure 4.3. In this simulation, the relaxation times are set to $T_1 = 3$ ns and $T_2 = 750$ fs.

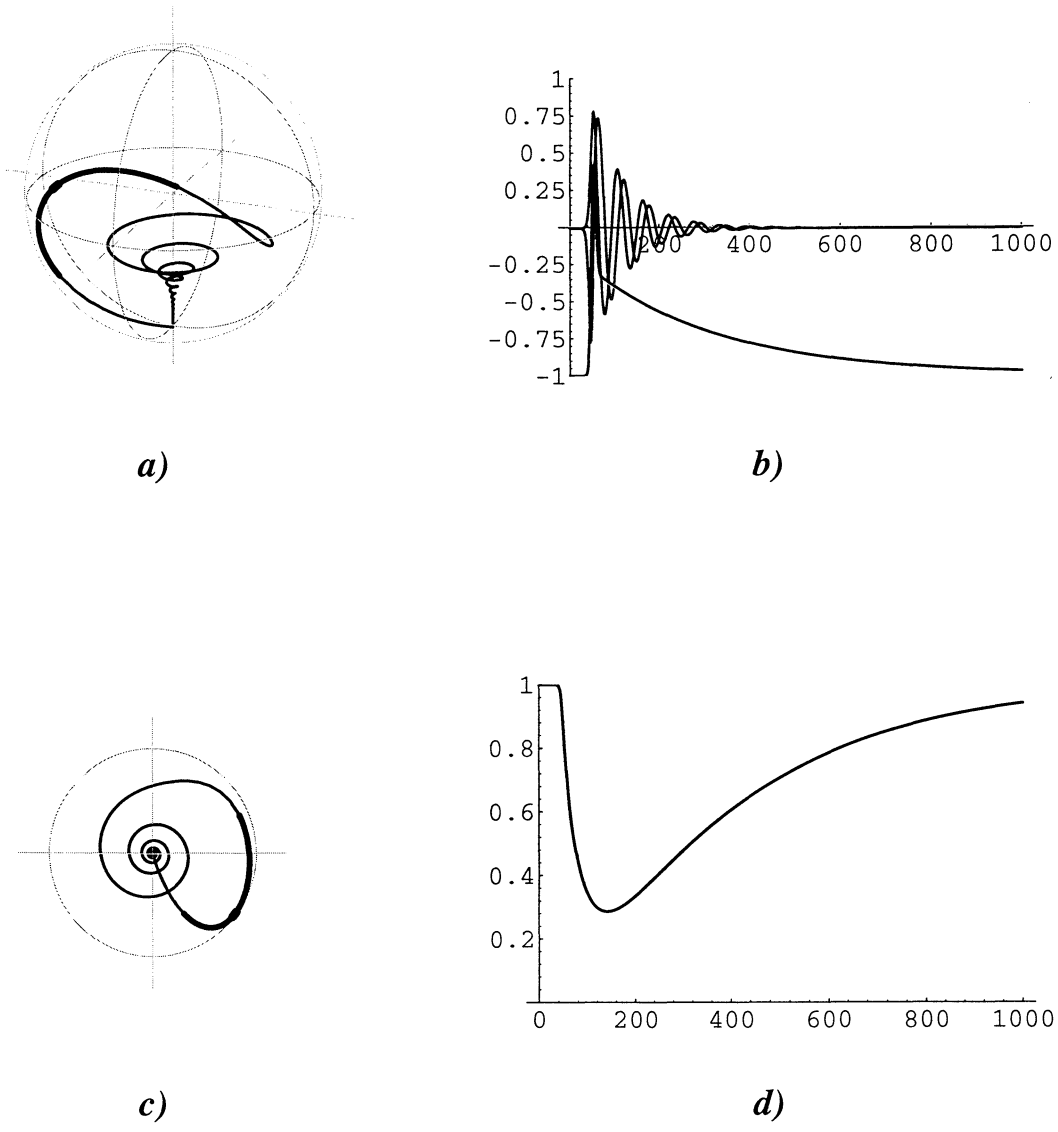

Figure 4.3: A simulation of how the Bloch vector is affected by the relaxation processes. Figure a) shows how the Bloch vector is moving in the Bloch diagram. b): How the Bloch vector's length in the u (green), v (red) and w (black) direction. c): Top view of figure a). d): How the absolute length of the Bloch vector is changing.

If the lifetimes Γ_1 and Γ_2' are very long, as for our cooled sample in our experiment, the significance of these factors in the Bloch equations is tuned down. The Bloch vector will instead move according to the other parameters. That means e.g. that if the electric field has moved the Bloch vector in such a way that it lacks a component in the w-direction, it will stay in this $(u, v, 0)$-plane. Because of the detuning factor Δ though, it will start to smear out like a fan in the (u, v)-plane. See figure 4.4. This happens since all the different molecules in our ensemble have slightly different excitation energies, due to individual surround-

ings, interaction with the matrix, etc. Because the Bloch diagram is rotating around the w-axis on the field frequency ω, a molecule excited with a slightly different frequency, ω_m, will have its own Bloch vector rotating on the detuning frequency $\Delta = \omega_m - \omega$, with respect to the coordinate system.

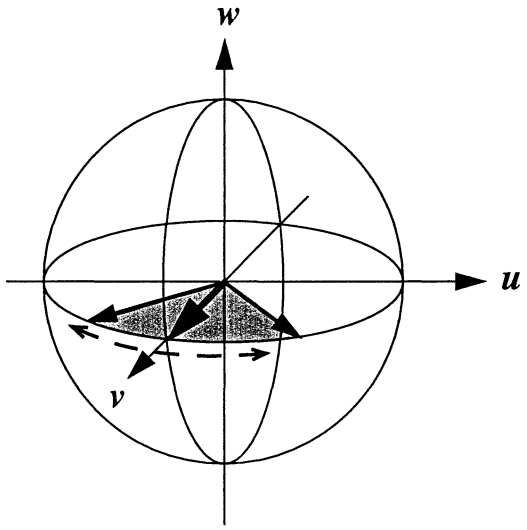

Figure 4.4: The Bloch vector starts to smear out in the (u, v)-plane, because of the slightly different excitation energies of the molecules in our ensemble.

4.1.3 Π- AND Π/2-PULSE EXCITATION

An electric field turns the Bloch vector around the u-axis by a certain amount of degrees depending on its integrated intensity. A $\pi/2$-pulse has therefore got its name from the fact that it is a pulse which causes the Bloch vector, see chapter 4.1.2, to make a $\pi/2$ rad (90°) turn around the u-axis. A π-pulse is thus, in a similar way, a pulse that turns the Bloch vector π rad (180°) around the u-axis, see figure 4.5, [ALL-87].

A $\pi/2$-pulse applied when all the systems are in the ground state therefore leads to an excitation, homogeneously spread over all the frequency components in the pulse, to a completely coherent state, compare with figure 4.5.

A π-pulse, on the other hand, applied under the same circumstances leads to a 100% excitation to level b of all the molecules, see the same figure. The area of

the pulse, that means, the electromagnetic field integrated over the pulse duration, determines the rotation angle of the Bloch vector.

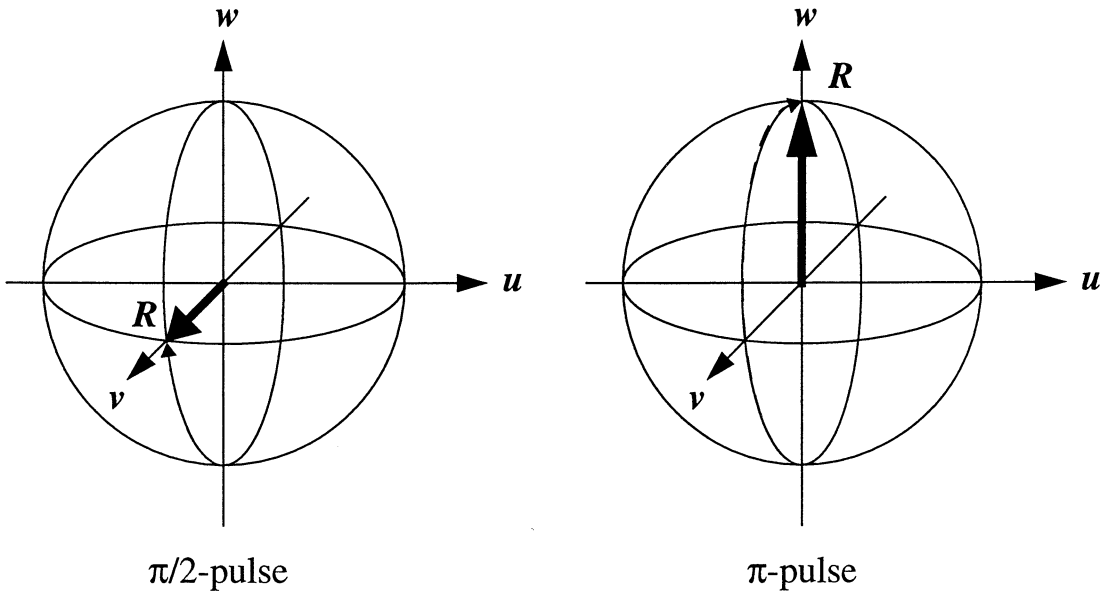

Figure 4.5: How the Bloch vector is turned when a $\pi/2$-pulse, respectively a π-pulse is interacting with the ensemble of molecules, all in the ground level.

If we first apply a $\pi/2$-pulse, and then directly afterwards, a π-pulse, we reach the situation shown in figure 4.6. We see that the π-pulse continues to turn the Bloch vector in the same direction around the u-axis.

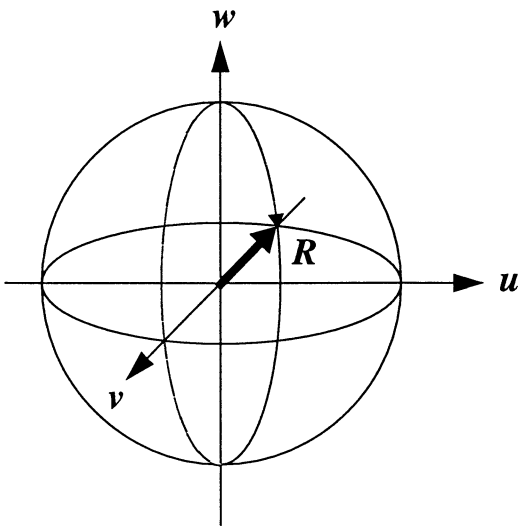

Figure 4.6: A π-pulse applied directly after a $\pi/2$-pulse. The π-pulse continues to turn the Bloch vector in the same direction as the $\pi/2$-pulse did.

4.1.4 TWO PULSE PHOTON ECHO

We observe that when our cooled material is being exposed to two, in time separated pulses, in the way later described in chapter 4.2, it responds by emitting an echo. The echo is emitted at the time τ after the second pulse, where τ corresponds to the time difference between the two pulses. This phenomena can be understood by representing the two pulses by a π- and a $\pi/2$-pulse and analysing their effect on the Bloch vector. To get an echo signal with as much intensity as possible, then theoretically, the first excitation pulse should be a $\pi/2$-pulse, and the second a π-pulse, which we will see.

In chapter 4.1.3 we saw that a $\pi/2$-pulse is defined as a pulse that excites all the molecules that have their resonant frequency within the pulse spectrum into a coherent state. We also saw that this was described in the Bloch diagram as a 90° turn of the Bloch vector around the u-axis, see figure 4.7a. All the excited molecules can be represented by such a vector which signifies that they have been excited into the same phase by the coherent source. In the same picture, the electrical field of the excitation is represented by an arrow along the u-axis. As it is proportional to the matrix elements describing the interaction with the system, it must point in the same direction as the real part of the off-diagonal elements in the density matrix.

During the time τ between the two excitation pulses, the excited states starts to dephase, due to their different excitation frequencies. This is shown in the Bloch diagram as a smearing out, like a sun-feather, in the (u, v)-plane, see figure 4.7b. Compare this picture with figure 4.8 of the race track, when the cyclists just have been started. The second excitation pulse is needed to act as the "ghost interrupter", telling all the cyclists to turn around and return back to the starting point keeping their original speed. This makes them all return to the starting point at the same time. The ideal pulse type for the second excitation pulse is thus a π-pulse. It turns all the individual frequency components 180° in the same direction as the $\pi/2$-pulse, around the u-axis, see figure 4.7c, so that the different Bloch vectors end up being flipped in the (u, w)-plane. When the individual Bloch vectors continue their movement in the (u, v)-plane, see figure 4.7d, they will actually recombine again after the time τ, just like the cyclists, and give rise to a macroscopic polarization, which results in a coherent output signal, see figure 4.7e.

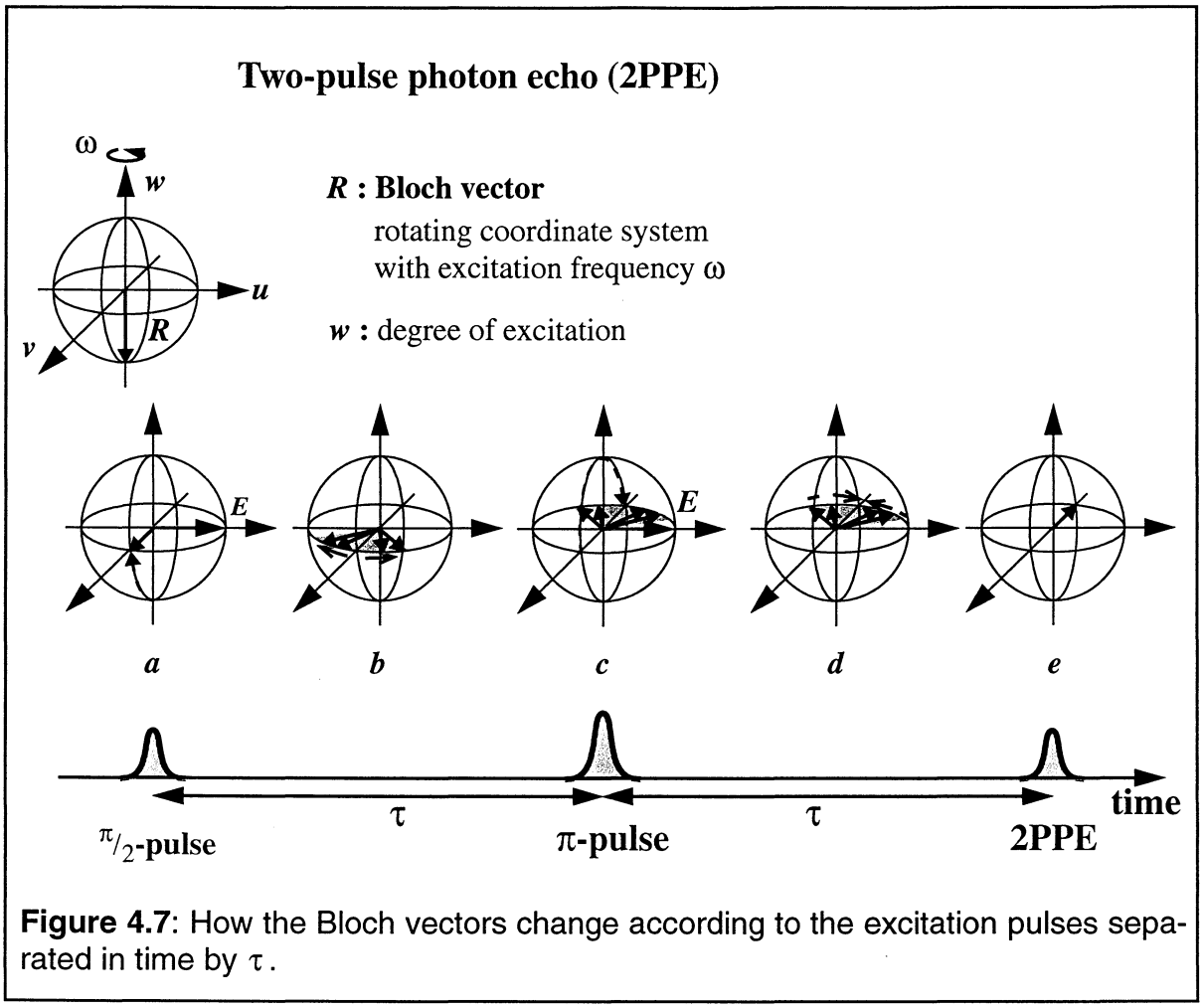

Figure 4.7: How the Bloch vectors change according to the excitation pulses separated in time by τ.

The direction in which the echo is emitted, $\vec{k}_e$, is determined by the wave vectors of the two excitation pulses, $\vec{k}_1$ and $\vec{k}_2$, according to the following equation:

$$\vec{k}_e = 2 \cdot \vec{k}_2 - \vec{k}_1 \tag{4.39}$$

See also figure 4.9. Here the index i = 1, 2 represents the time order of the two excitation pulses. In the experiment an angle of 3.6° between the two excitation pulses was used. The advantage of this is a background free detection of the echo signal. We conclude from equation (4.39) that when the time order of the two excitation pulses are changed, the diffraction of the echo will occur in an other direction, corresponding to the dashed line in figure 4.9. I will give the two directions names, depending upon which excitation pulse that hits the sample first. When the reference pulse is first, then the echo appears in the 1^{st} diffraction order, and when the reference pulse comes as second pulse, the echo appears in the -1^{st} diffraction order.

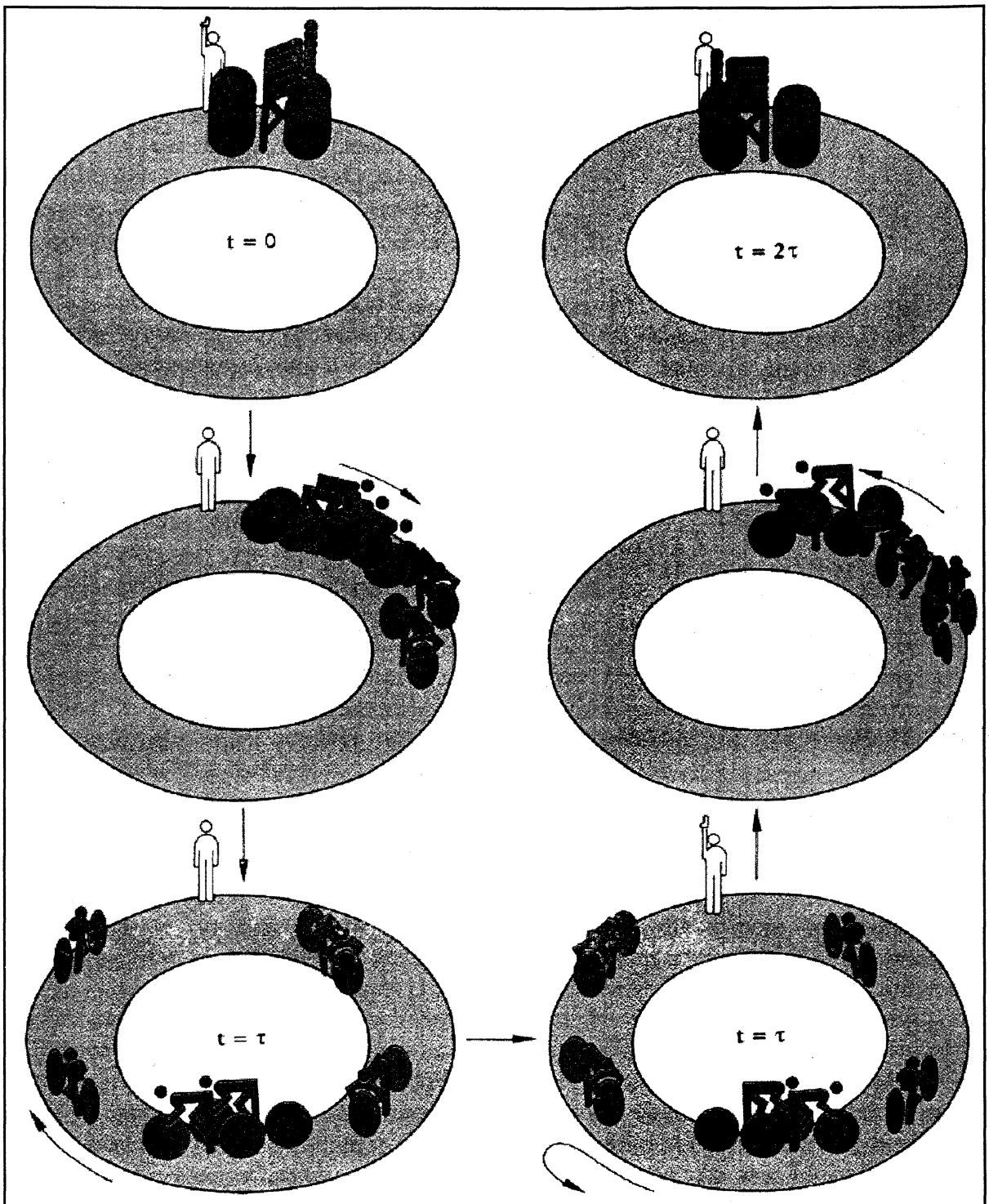

Figure 4.8: The cyclists, all starting at the same time and with an individual constant speed (the $\pi/2$-pulse). After the time τ, the starter signals to them all to change direction and head back to the starting point again (the π-pulse). They return back with the same individual speed as before, returning all at the same time at the finishing line the time τ after the return signal, establishing the echo. Figure found in [BLÜ-90].

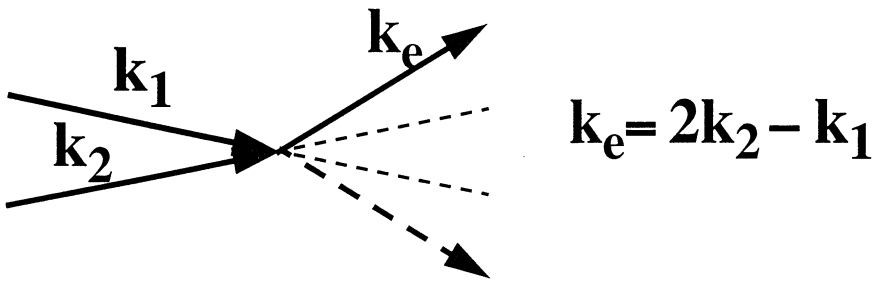

Figure 4.9: The echo is admitted in the above shown direction. The direction is given by the two excitation pulses wave vectors. If the temporal order of the two writing beams is changed, the echo is emitted in the direction implied as a dashed arrow above.

Equation (4.39) has the form of a momentum conservation criterion. It can be obtained by calculating the direction of the emitted radiation of the polarization created by pulse no 1 and 2 in the sample. On the other hand, we have seen that the Bloch equations are linear in frequency, i.e. that they don't describe any interaction between different frequency components. Since the wave vectors are proportional to $1/\lambda$, we see that the linearity of the Bloch equations and equation (4.39) can only both be fulfilled if the angle between the two excitation beams are 0°. If the angle is not zero, the equation (4.39) implies the variation of the echo frequency from those of the excitation. The Bloch equations can't explain this. If the mixing of frequency components is allowed to happen, then a shift of the echoes spectrum must occur for large angles. This has been experimentally observed, and a different model has been proposed to describe this phenomena [ZUI-96]. On the other hand we can regard equation (4.39) to be phenomenological, i.e. that it is good for small angles, and that we will find an echo signal in the experiment in the $\hat{k}_e$-direction. For small angles though, no changes in the echo spectrum is observed either.

If the intensities of the excitation pulses are low, (i.e. if the pulse areas are small compared with $\pi/2$), two pulse photon echoes could be described similarly to the accumulated photon echo, by a linear approach [SAA-86]. The model treats the sample as a spectral-spatial-domain filter, where the electric field strength of the echo in the spectral domain, $E_e(\omega_i)$, only depends on the excitation fields, at the same frequency, ω_i, and not on the excitation fields at the other frequencies, $E(\omega)$ where $\omega \neq \omega_i$. The advantage of the linear description is that it permits to find the amplitudes as well as the phases of the echo signal by simple calculations. According to the linear approach, the electric field strength of the 2PPE is given by:

$$E_{Echo}(\omega) \sim E_1(\omega) \cdot E_2^2(\omega) \tag{4.40}$$

where $E_1(\omega)$ and $E_2(\omega)$ are the electric field strengths in the first and in the second pulse, respectively. For intensity spectrum components, $I_e(\omega)$, of 2PPE the similar relation is valid:

$$I_e(\omega) \sim I_1(\omega) \cdot I_2^2(\omega) \tag{4.41}$$

Equation (4.40) and (4.41) are the explanation for finding only those frequency components in the echo signal which are present in both the excitation pulses. It shows again the linearity in the frequency domain implied by the Bloch model.

From equation (4.41) we see that the echo's intensity for a certain frequency is also dependent upon the temporal order of the excitation pulses. The only time that a change in the temporal order don't changes the intensity of the echo signal in the two directions, is when the same frequency components in both excitation pulses have equal intensity.

Since equation (4.40) is only valid for low intensities, the maximum intensity of the echo signal (for $\pi/2$- and π-pulses) can never be optimized anyway. So what happens with our Bloch vector model when the two excitation pulses do not correspond to a $\pi/2$- and a π-pulse respectively? We have seen that the electric field turns the Bloch vector by some degrees in the (v, w)-plane. But regardless of how much the Bloch vector has been turned in the Bloch diagram, see figure 4.10, it can always be split into a component in the (u, v)-plane, and a component in the w-direction. Thus, there are always some molecules that have experienced the pulse as if it was a $\pi/2$-pulse. The same is true for the second pulse. There will always be molecules that experience it as a π-pulse, and thus there will always be an echo, regardless of whether or not one has optimized the experiment so that the first is a $\pi/2$-pulse, and the second a π-pulse, except when both the pulses are π-pulses. By not optimizing the pulses intensities that we excite our sample with, the intensity of the echo will be lower than optimum though, but on the other hand is multiplication of the two pulses possible.

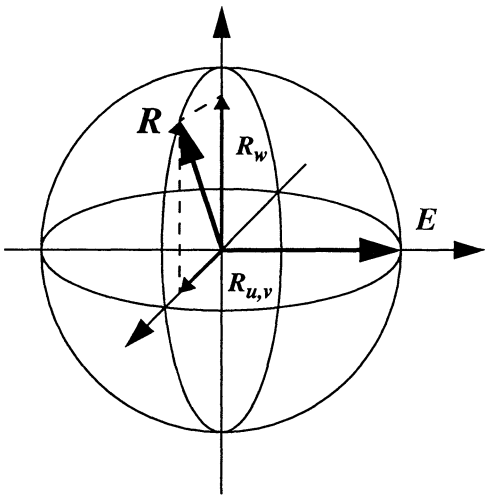

Figure 4.10: The applied pulse is no $\pi/2$-pulse, but it has a vector component in the (u, v)-plane, and thus does some of the molecules experience the pulse as a $\pi/2$-pulse.

4.2 EXPERIMENT

In order to answer the question asked in the introduction, we have to perform a two pulse photon experiment, where the two excitation pulses have different spectra. This implies two different experimental approaches discussed below.

4.2.1 MODULATION OF ONE EXCITATION PULSE

For the modulation of one of the excitation pulses, the pulse was split by a beam-splitter. One of the beams was directed into the modulator, the object pulse, and the other, the reference pulse, into a delay line corresponding to the average length that the other pulse travels through the modulator, see figure 4.12. In the modulator, a liquid crystal array was placed in the FP providing different modulation patterns, according to the description in chapter 3.2.2.

4.2.2 MODULATION OF BOTH EXCITATION PULSES

In order to modulate both excitation beams, the initial beam is split into two, by a beamsplitter. The two beams are made parallel and guided into the modulator at different heights. The vertical separation of the beams is large enough in order to modulate them independent of each other, see figure 4.11. Thus, we have also modulated the reference pulse. In order to distinguish them from each other, the pulse that passes the upper way through the modulator will be called the object pulse, and the one that takes the lower path, the reference pulse. The definition of the echo's directions, will thus be the same as given in chapter 4.1.4.

As the horizontal plane is a symmetry plane for the modulator setup, the two beam paths are equivalent. Therefore, with no mask in the FP, the resulting pulses should be the same for both beams, which was verified experimentally.

As our LCA does not have another array section in the vertical direction, which allows to be addressed individually for a different amplitude pattern, we need to use a simpler method. Instead we placed two slides with different patterns in them, above each other in the Fourier plane, see figure 4.11. This allowed us to modulate the two beams independently. By using different patterns at the two positions, and moving them perpendicular to the beam, we could achieve different modulations of the two excitation beams.

For this experiment we tried to make the patterns in the two empty slide frames as identical as possible. Four copper wires, each with a diameter of 0,2 mm and with a distance to the next wire of circa 0,6 mm, were placed vertical and parallel to each other in each frame. The bar masks were placed above each other in the modulator so that their patterns overlapped in such a way that the frequencies blocked by the wires in one of the masks were not blocked by the other mask. The spectra of the excitation pulses can be seen in figure 5.2 in chapter 5.3.

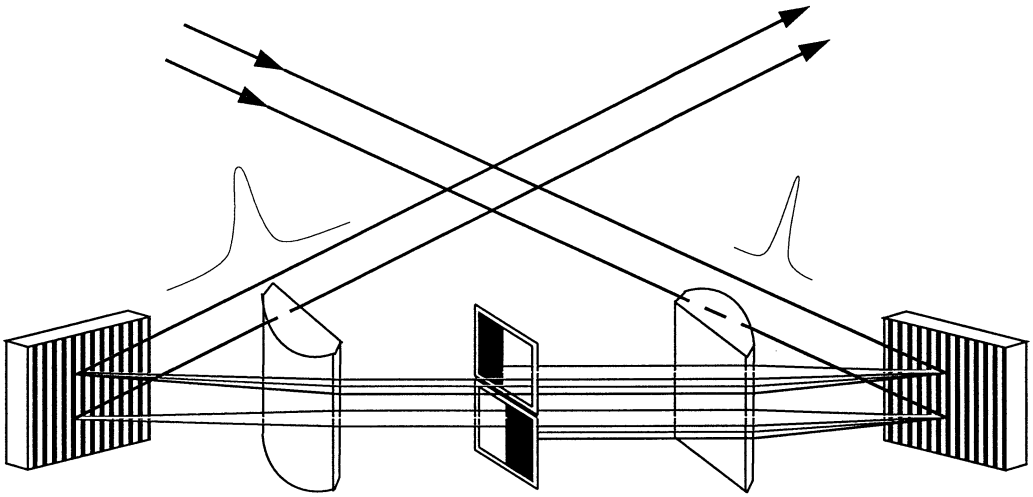

Figure 4.11: Modulation of two input beams in the modulation setup.

4.2.3 EXPERIMENTAL DETAILS

In the experiment, we expose a sample made of organic dye molecules in a polymer matrix to two pulses, separated in time. One or both of the two pulses are spectrally modulated, as described in chapter 4.2.1 and 4.2.2. The sample responds by emitting an echo, at the time τ after the second excitation pulse, where τ corresponds to the time delay between the two excitation pulses. The direction in which the echo is emitted, is given by equation (4.39) in chapter 4.1.4. The experimental setup is shown in figure 4.12.

For our experiment, we use the femtosecond Titanium:Sapphire laser system CPA 1000 described in chapter 2. This provides pulses with an intensity high enough to excite photon echoes efficiently. The ultra short pulses provide a broad spectrum which can easily be modulated using SLM's, (chapter 3).

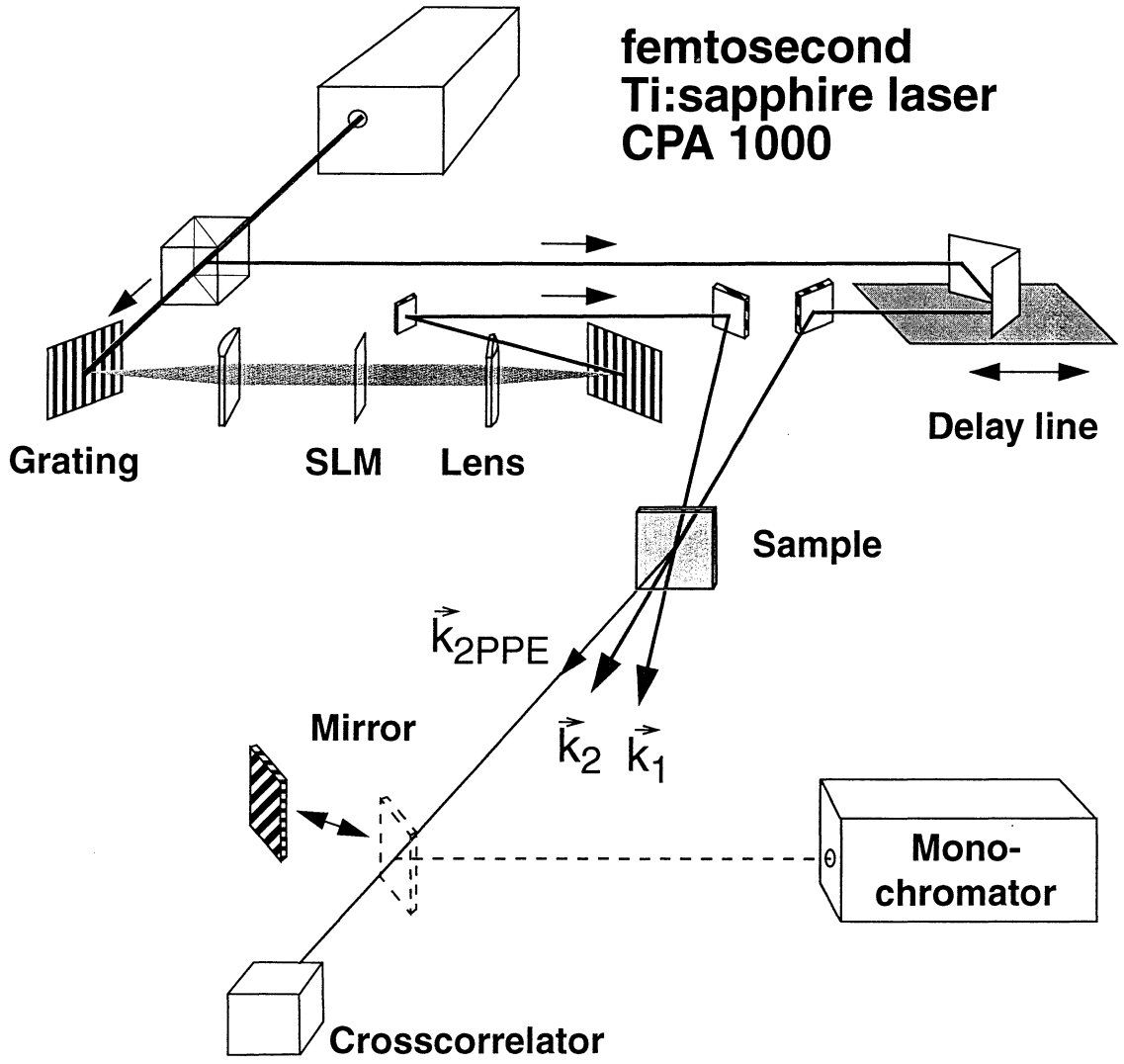

Figure 4.12: The whole experimental setup for modulation of one of the excitation pulses.

The sample is a circa 100 µm thin film, (lateral geometry 2*2 cm), produced from polyvinylbutyral and doped with molecules of a zinc-naphthalocyanine dye (Ciba 3463) at a concentration of 10^{-3} mol/l. The absorption spectrum of this material at room temperature is shown in figure 4.13. We can see that the peak of the inhomogeneously broadened absorption band is at 770 nm and that the FWHM value of the band is about 40 nm. With respect to the experience made with several similar compounds, the inhomogeneous band hardly depend on the temperature, i.e. the low temperature spectrum is expected to be very close to figure 4.13. At the absorption maximum, the optical density (O.D.) of the sample is 1,7.

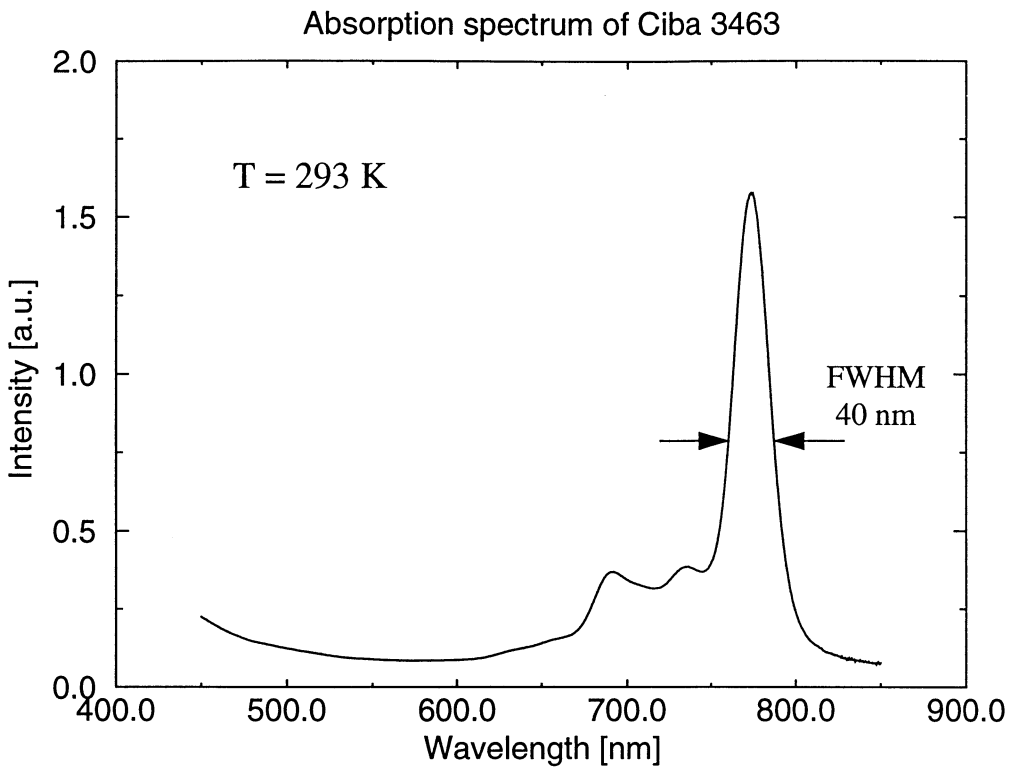

Figure 4.13: The absorption spectrum of the sample used for these experiments. The sample is made up of polyvinylbutyral, doped with molecules of a zinc-naphthalocyanine dye (Ciba 3463).

In order to increase the coherence decay rate T_2' (see chapter 4.1.1), the phonon interaction must be reduced drastically. Therefore, the sample is cooled down to cryogenic temperatures. The sample is immersed in liquid helium in an optical bath cryostat. The cryostat used is a handy UTREX-A2 ("Sputnik", Ukraine) which allows cooling to 2 K within about 2 hours. First the nitrogen chambers are filled with liquid nitrogen, and thus cooled to the temperature of 78 K. Between the nitrogen and the helium container there is a vacuum chamber, that guarantees a good thermal isolation. When the cryostat has been cooled to the liquid nitrogen temperature, the cryostat is filled with liquid helium (4,2K). By pumping the helium chamber, the temperature is decreased to 2 K (below the λ-point), at which the helium is in a super fluid state.

Independent upon whether one or two of the excitation beams were spectrally modulated, the two 2PPE-experiments are carried out the same way. The two excitation spectra are measured with a monochromator. To destroy the spatial appearance of the pulses, we placed a diffuser in front of the slit to the monochromator, in the cases where we had enough intensity to do so, e.g. for the excitation pulses. The excitation amplitude in the time domain are determined by measuring

the crosscorrelation of the pulse with a reference pulse that hasn't passed through the modulator.

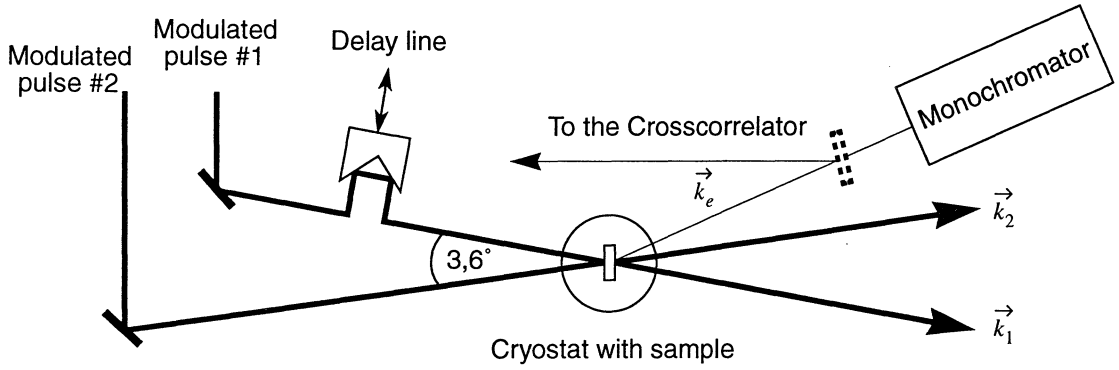

Figure 4.14: The setup to create and detect the two pulse photon echo.

The two excitation beams overlap at the sample under an angle of ca 3.6°, see figure 4.14. The intensity of the echo depends on the time delay, τ, between the two excitation pulses, on their intensities and on the amount of their spatial overlap on the sample.

In the case where one of the beams was modulated with the help of the LCA, we recorded the spectra using the monochromator and a CCD-array connected to an oscilloscope. When all measurements that were depending on each other have been made, we recorded a calibration spectrum, by scanning the monochromator. The reasons for not using the monochromator for the spectral measurements were two. Firstly, the monochromator has a random fault of circa 0,5 nm which originates from the scanning mechanics, see chapter 6.5. The scan-free measurement with the CCD-array does not have this drawback. But the scale on the CCD-array was unknown, so we had to make one calibrating spectrum scan. But by only scanning once, the formerly performed spectral measurements that depended upon each other, have at least the same random spectral shift. The second reason was the advantage of saving time by using the oscilloscope.

For the experiment with two modulated excitation beams, we measured both the spectra and the time profiles of the echoes. The spectra were measured by scanning the monochromator without a diffuser placed before it, since the intensity of the echo was too low. The time profile was measured by performing a crosscorrelation with an unmodulated reference pulse (as for the time resolved measurements of excitation pulses).

5 RESULTS AND DISCUSSION

5.1 THE ECHO INTENSITY DEPENDENCE OF THE TIME DELAY BETWEEN THE EXCITATION PULSES

We measured the intensity and spectrum of the echo for different time delays between the excitation pulses, τ, when the spectra were not modulated. Near the zero-delay, (time delay: $|\tau| < 200$ fs), we observed high intensity echo signals. This can be explained by the fact that also states that are affected by the broad band phonon interaction can contribute to the echo formation at this timescale. The coherence of excited states interacting with phonons, decay with the phonon lifetime, which is in the order of some 100 fs. Therefore, those states can not contribute to the echo formation at a time exciting this limit. In analogy we can say that only the zero phonon line of the homogeneous spectrum is responsible for the echo at long timescale. For short time delay, τ, however, the echo intensity is increased by the contribution of the states with phonon interaction. The amount of this increase should correspond to the ratio of the zero phonon line to the phonon sideband in the homogeneous spectrum. As a consequence of the broad band phonon interaction, the spectrum of the photon echo at zero delay, is thus more complicated than for longer time delays. To simplify the analysis of our experimental results, we therefore later chose to work at delays $\tau \gg 200$ fs, but yet much shorter then the coherence decay rate, T_2'.

5.2 MODULATION OF ONE EXCITATION PULSE USING AN LCA

The pulse from the amplifier was split into one reference pulse and one object pulse that passed through the setup to be modulated by the LCA, as described in chapter 3.2.2.

The LCA was programmed with different rectangular functions, and the total time average continuous wave intensity of the reference pulse and the unmodulated object pulse were both set to 30 mW. The spectra of the echoes in both

directions and of the excitation pulses for these patterns were recorded. Some of the results from these measurements are shown in figure 5.1. The graphs, **A** to **D** show different spectral modulations. The labels for the spectra are ① for the modulated excitation pulse ② for the echo in the 1^{st} and ③ for the echo in the -1^{st} diffraction order (chapter 4.1.4), respectively.

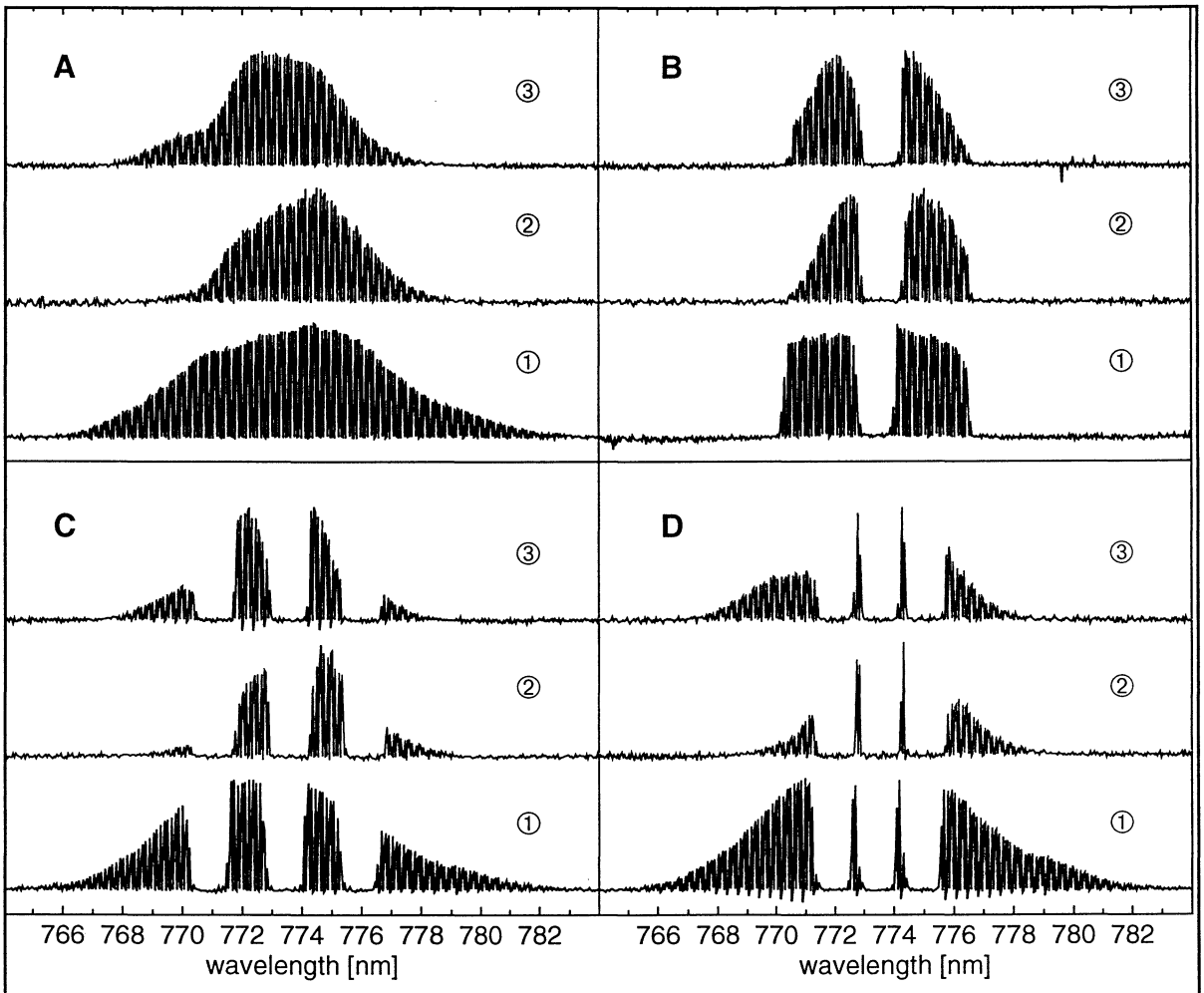

Figure 5.1: Amplitude modulation of the spectra of excitation and echo pulses. Spectral modulation of one excitation beam (①) causes the same modulation in the spectra of the echoes in the 1^{st} (②) and -1^{st} (③) diffraction order.

The graph **A** shows the spectra of the unmodulated excitation pulse that went through the setup, ①, and of the echoes in the two directions, ② and ③. We see that when the sample is excited by two unmodulated pulses, the echo spectrum does not correspond well to that of the excitation, see figure 5.1. This can be explained by that the pulse has not fully been transformed back during its passage from the Fourier plane and out of the modulator. We thus have a pulse with an inhomogeneous spectral distribution in its beam profile.

This was verified experimentally by observing the change in intensity over the beam profile after the modulator, when more and more of the spectral components were blocked in the Fourier plane. By eye we saw a clearly non uniform change of the spatial intensity distribution. We therefore conclude that a pulse that passes through the modulator setup is not fully transformed back into a mode with homogeneous distribution of all frequency components. When the object pulse and the reference pulse overlap at the sample, some of the frequency components can be missing in the area of the overlap region, and others can be over represented. The ratio of intensity of a given spectral component in the two excitation pulses also shows an inhomogeneous spatial distribution in the overlap region. Because of the asymmetry of equation (4.40) chapter 4.1.4, with respect to the temporal ordering of the excitation pulses, the echo spectra in the two different orders do not need to be identical. In fact, we observe asymmetric echo spectra in case of unmodulated excitation, spectra ① and ② in **A**, as well as asymmetric spectral envelopes in all of the following modulations, **B**, **C** and **D**, in figure 5.1.

5.3 MODULATION OF BOTH EXCITATION PULSES USING TWO BAR MASKS

To spectrally modulate both excitation pulses, the pulse from the amplifier is split into two, and directed through the modulator at different heights. By placing two masks with certain patterns at different height in the Fourier plane, as described in chapter 4.2.2, an independent modulation of the pulses is achieved. The pulses in the upper and lower beam are named object and reference pulse, respectively.

For this experiment we produced two bar masks, made as identical as possible. Each mask consists of an empty slide frame, in which four copper wires were fixed, as described in chapter 4.2.2. The spectra of the reference pulse and the object pulse are shown in figure 5.2 as ① and ②, respectively. By this type of modulation, we expect an echo spectrum with eight dips, according to the multiplication of the two excitation pulses, ⑤, shown in the same figure. This is what we actually found in both directions. The echo in the 1^{st} and -1^{st} diffraction order are represented with ③ and ④, in figure 5.2, respectively.

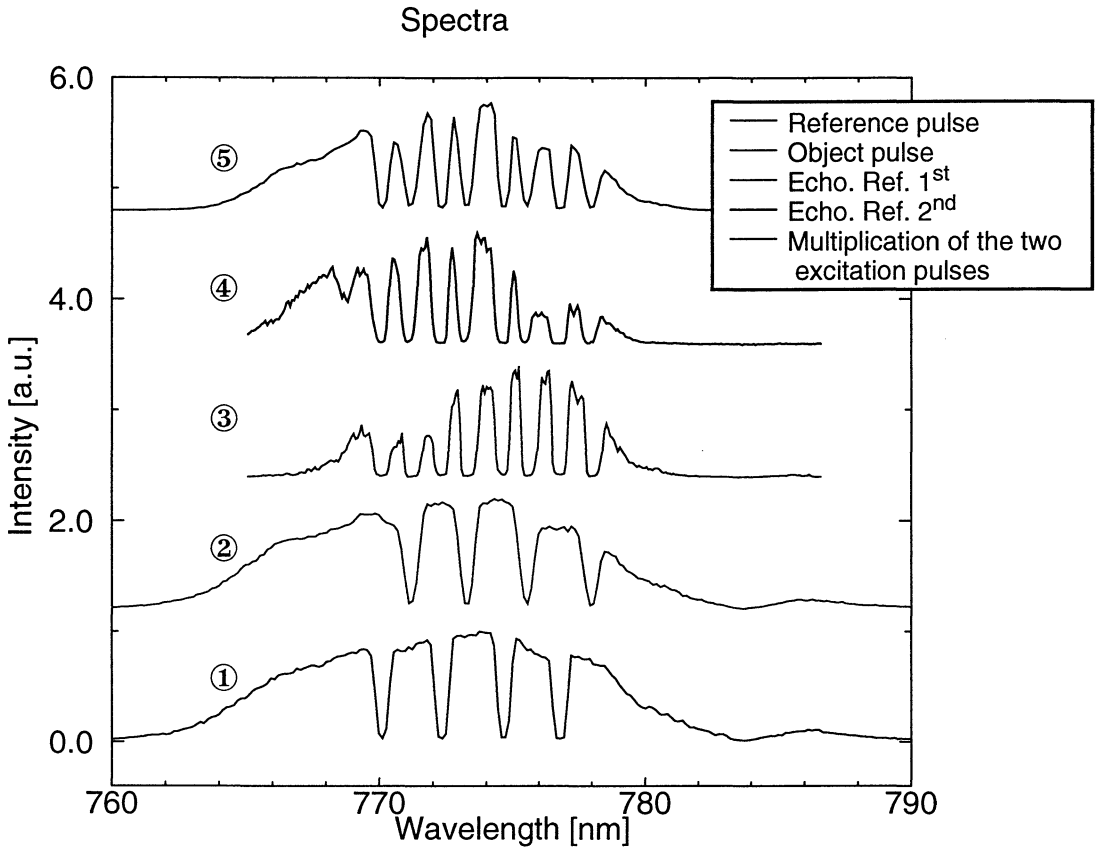

Figure 5.2: Spectra of the modulated excitation pulses, the echo spectra in both directions and the multiplication of the two excitation spectra. We see that the echo spectra are only made up by the frequency components that exist in both the excitation beams, and look very similar to the multiplication of the two modulated excitation pulses.

The asymmetrical spectrum of the echo in the -1^{st} diffraction order, ④, is most likely due to accidental changes of the wires positions in the masks during the measurements.

These results were achieved when the intensity of the excitation pulses were reduced to 22 mW for the object beam and 26 mW for the reference. For the echoes in the 1^{st} diffraction order, spectral measurements of the echo at higher intensities of the excitation beams (65 mW for the object beam and 77 mW for the reference) and at lower intensities (12 mW for the object beam and 14 mW for the reference) were also made. This was done to make sure that we are working in the linear regime where the equation (4.40) is valid. The results from these measurements are presented in figure 5.3. We see that for the two lower excitation intensities the spectra corresponds well to our expectations, while for high intensities, the echo spectrum differs from the pure multiplication of the two

excitation spectra. The dips in the spectrum are filled up to a higher extent, i.e. the echo spectrum now contains spectral components which were present in one of the excitation pulses only. Thus, for intensities above a certain value, the linear approach leading to equation (4.40) is no longer valid. In conclusion, in order to carry out correct spectral domain multiplication, we should work at low intensities.

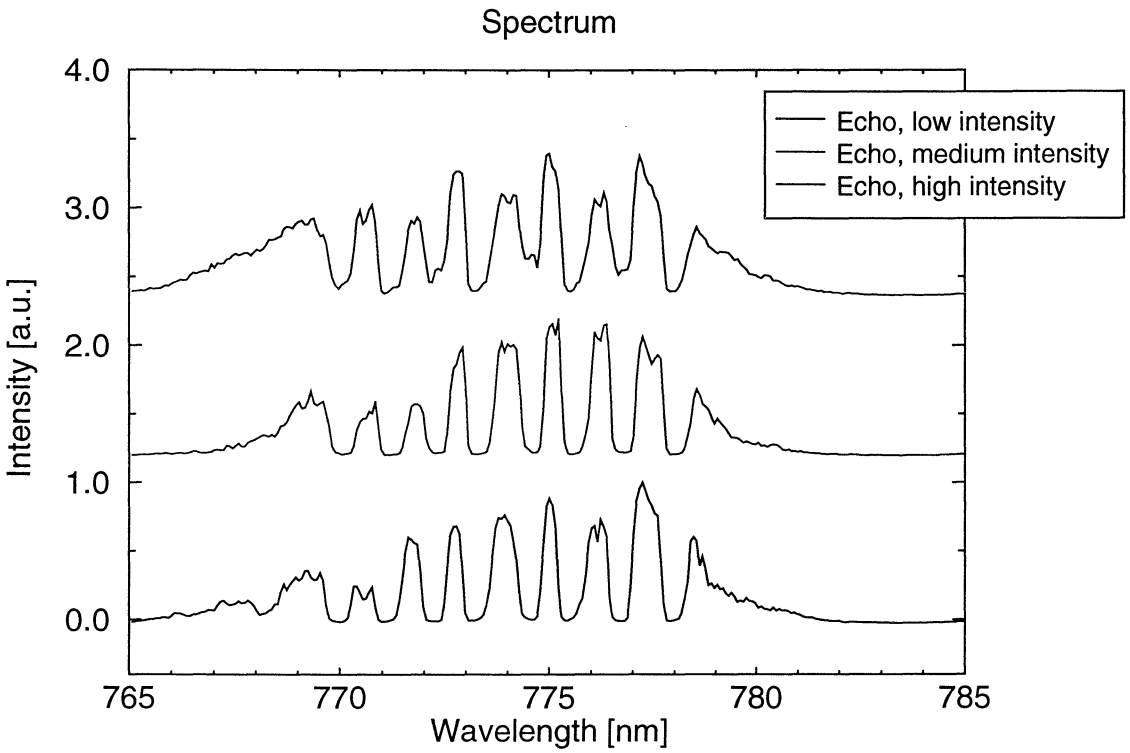

Figure 5.3: Echo spectra in the 1st diffraction order at different intensities of the excitation beams. The high intensity excitation does no longer correspond to the linear regime and thus the echo spectrum differs more and more from the net multiplication of the excitation spectra.

5.4 TEMPORAL MEASUREMENTS OF SPECTRALLY MODULATED PHOTON ECHOES

We performed time resolved measurements of the excitation pulses and of the echo by crosscorrelation with a reference pulse, split off before the modulator setup. The spectra of the excitation pulses and the corresponding crosscorrela-

tions can be seen in figure 5.4. In the same figure, a spectrum similar to that of the excitation pulses has been simulated and is shown above the experimental data, ①. The crosscorrelation trace of the pulse corresponding to this spectrum was calculated too and is shown, ②, on top of the right column in figure 5.4. In order to do this, we made the assumption that the phase for the excitation pulses does not change when passing through the mask in the setup, and therefore set the phase to zero. The spectrum ① was multiplied by the spectrum of a simulated reference pulse, and the product was Fourier transformed into the time domain. The simulation of the crosscorrelation trace fits quite well with the experimental data. The temporal separation, τ, of the satellite peaks corresponds to the inverse distance of the dips in the spectrum. However, the ratio of the peak intensities is not well reproduced, as well as the width of the pulses. This will be discussed below. On the other hand, the position of the dips in the spectrum hardly affect the simulated crosscorrelation, as one may would expect. The asymmetry in the crosscorrelation for the lower pulse is probably due to detection problems, rather then a correct result.

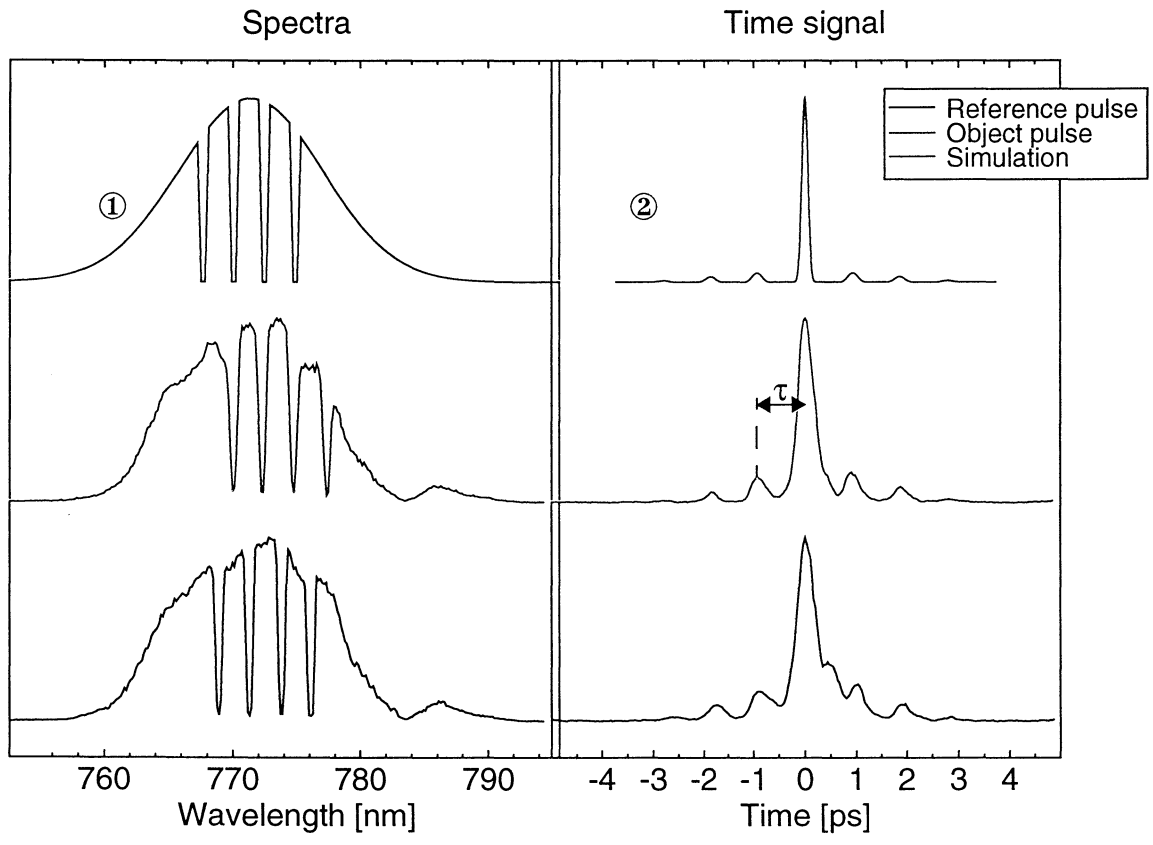

Figure 5.4: The measured and the simulated spectra and time signals of the excitation pulses.

The spectra and crosscorrelation of the echo in the 1st diffraction order are shown in figure 5.5. The intensity of the excitation pulses was about 25 mW. Above the experimental data, a simulated echo spectrum, ①, and a simulated crosscorrelation, ②, are shown. We see that the simulated crosscorrelation is again quite similar to the measured ones. The time distance between the central peak and the closest satellite, is twice as long for the echo signal as it is for the excitation pulses. This is in agreement with the decrease of the distance between the dips by a factor of two with respect to the excitation spectra. The differences in intensity and the width of the peaks can be attributed to at least four things. Firstly, the simulated spectrum has a slightly larger FWHM than that measured in the experiment. The simulated crosscorrelation should thus have a narrower peak width. Secondly, the reason for the different intensity ratio between the central peak and the satellite peaks in the experiment and in the simulation may be due to saturation of the detector at the central peak. We later performed new crosscorrelation measurements with lower excitation intensities and got better agreement with the simulations. For the third, the phase may be changed by the mask, so putting the phase to zero in our simulation may not be correct. And last but not least, the excitation pulses may not be transform limited, as we have seen in chapter 2.4. Thus the measured time signals must not fully correspond to the Fourier transform of the spectra.

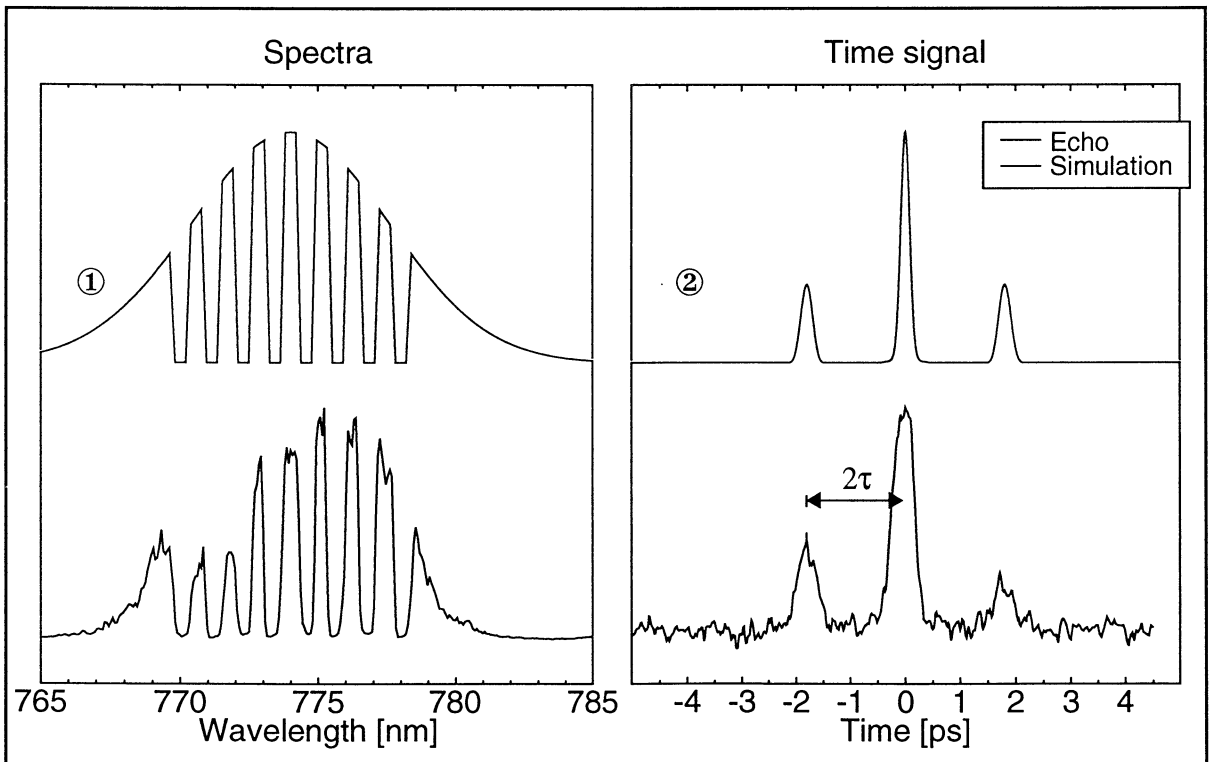

Figure 5.5: The measured and the simulated spectra and time signals of the echo in the 1st diffraction order

5.5 DISCUSSION OF ERROR SOURCES

We observed a random frequency shift of our monochromator. To check this, we made ten measurements of the emission spectrum of a HeNe-laser, at a very slow scanning speed of the monochromator. A diffuser was placed before the entrance slit of the monochromator to scatter the light. The wavelength of a HeNe-laser is known to be 632,8 nm. The measurements are shown in figure 5.6. Note that the starting-point and speed of the monochromator scan was the same within operator handling precision. Nevertheless, we get ten different emission peaks. We conclude that our monochromator has an internal offset of circa -1,2 nm and a random error of about 0,5 nm.

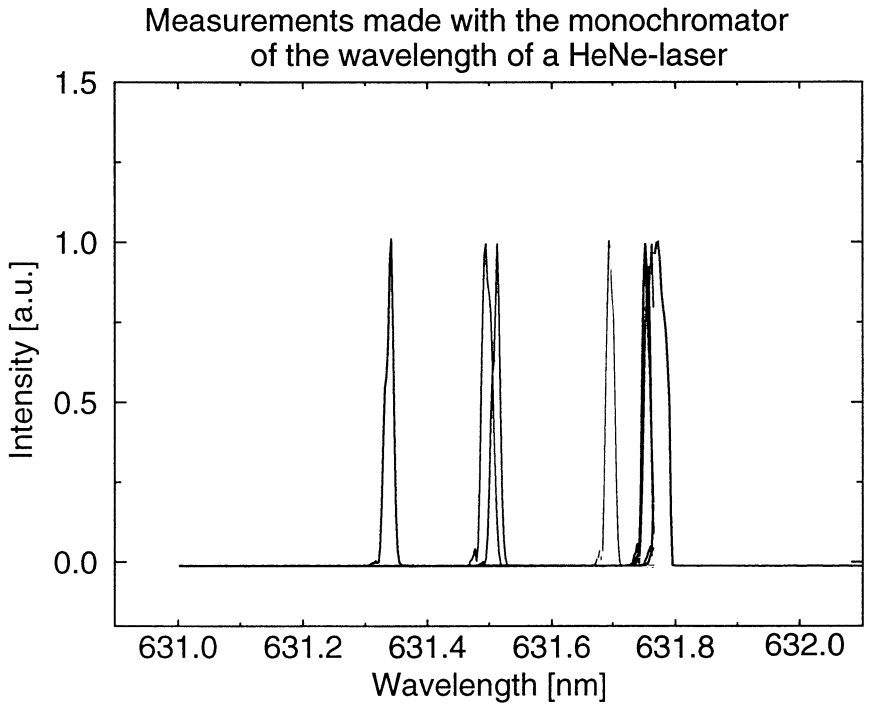

Figure 5.6: Ten measurements of the emission wavelength of the HeNe-laser with identical parameters for the wavelength scan of our monochromator. We see that the monochromator has a random error of circa 0,5 nm and an internal offset of about 1,2 nm.

The synchronisation of the scan of the monochromator and the data acquisition with a PC is done manually. The resulting frequency shift is therefore proportional to the reaction time of the operator (me!). The error here can be as big as 0,1 nm.

As the excitation beams have an inhomogeneous distribution of frequency components across the beam profile, the echo will have that too. To average this distribution, the use of a diffuser before the entrance slit of the monochromator would have been necessary. This was not possible on account of the low intensity of the echo signal. Therefore, the measured echo spectra depend on the coupling into the monochromator, which can not be reproduced perfectly.

The local heating of the sample due to the high intensity of the excitation pulses can lead to boiling of the helium. Diffraction on the bubbles lead to random changes in the echo intensity during the measurement of the spectrum. To avoid this, we always blocked the excitation pulses before the cryostat when no measurements were made.

The dye molecules in our sample are chosen to have a low tendency to be affected by spectral hole burning, SHB. The contribution of SHB to the echo signal has been measured, and is in the order of 10%.

The grating in the modulator are rather old and partly damaged, which can be seen by eye. This damage may cause some amount of incorrect dispersion.

6 CONCLUSIONS

6.1 BIT MULTIPLICATION IN THE SPECTRAL-DOMAIN

Our experimental data demonstrate that, in the limit of low excitation intensities, the structure of the echo spectrum can really be described in terms of a multiplication of the spectral components of the excitation pulses. In the experiments where only the object pulse was modulated, the echo spectrum exhibits the same structure as the object pulse, whereas in the second type of experiment with both pulses carrying spectral modulation, the echo inherits the structure from both. However, if the echo spectra in the two different diffraction orders are compared with the structure expected according to equation (4.40), we observe a narrowing and an asymmetry of the spectral envelope. We have experimental evidence that this result is due to a slight misalignment of our modulator setup which leads to a non-uniform intensity distribution of the frequency components across the beam profile. With an ideally operating modulator, however, the echo spectra are at least expected to be symmetric in both diffraction directions.

Despite of this asymmetry of the envelopes the main experimental goal is achieved. The structure of the echo spectrum corresponds to a formal multiplication of the excitation spectra, i.e. only those spectral components are present in the echo which do not vanish in either of the excitation pulses. This is true for moderate excitation intensities, for which the linear approach that lead to equation (4.40) applies. The experiment shows the failure of this linear model if the excitation intensity is too high.

Based on these properties of the photon echo spectrum we can interpret the experiment as an implementation of a multiplication in the spectral domain[1)]. We were able to establish eight spectral dips of finite size in the echo spectrum which can be easily detected by conventional spectrally selective detection methods. If we measure the signal intensity at the frequency position of the dips only and

1. To our knowledge, all the nano- to femtosecond time scale photon echo data processing experiments, which have been done so far, use temporal domain processing, where the similar data multiplication is not feasible. It has been performed in the mikrosecond time scale though [KRÖ-93]. Here, the dividing into the spatial and spectral domain processing is not absolute as the spectrum and temporal shape of an optical signal is not independent. It indicates in which domain the data are decoded and detected.

assign "zero" to intensity values smaller than a given threshold and "one" to higher values, the echo spectrum corresponds to the eight-bit vector (0,0,0,0,0,0,0,0). In analogy, the excitation pulses represent the vectors (1,0,1,0,1,0,1,0) and (0,1,0,1,0,1,0,1), respectively (see figure 6.1). The vector represented by the echo spectrum is equal to the product of the vectors corresponding to the excitation pulses. We can use a general formulation by writing

$$A_i^{OUT} = A_i^{IN1} \cdot A_i^{IN2}$$

where A_i is the i^{th} bit of the output or the input vector, see figure 6.1. The upper index OUT, correspond to the output vector, the echo, and the indexes IN1 and IN2 to the temporal order of the input vectors, the excitation pulses. The bits, A_i, can have two values: 0 or 1. This means that we can carry out the femtosecond time scale multiplication of the input information coded into the excitation spectra at a repetition rate of 1 kHz.

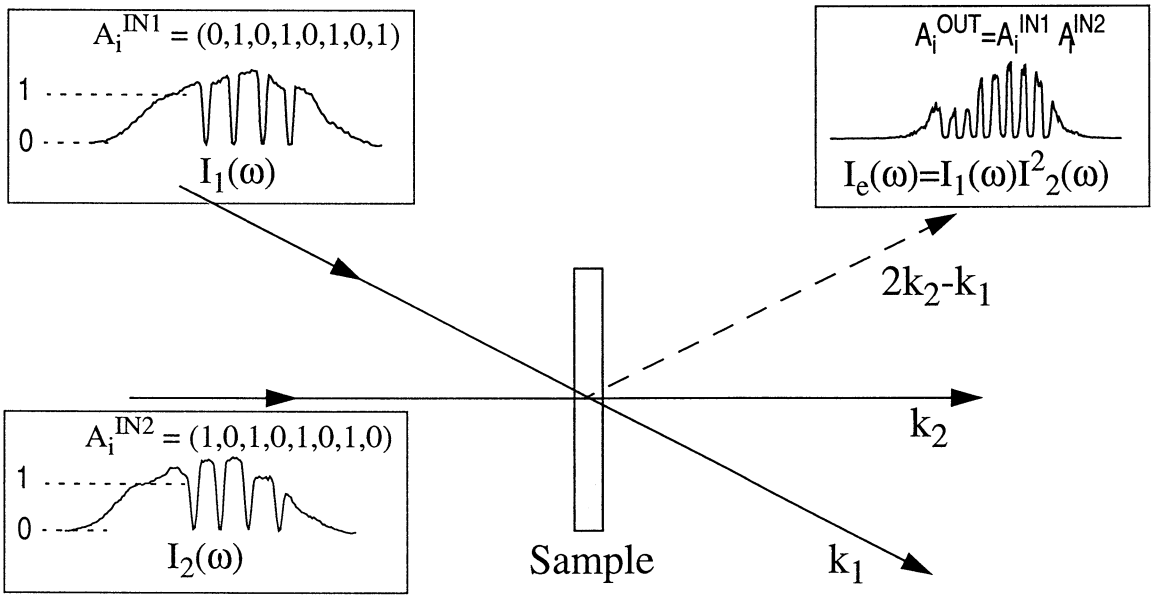

Figure 6.1: Spectral multiplication by femtosecond 2PPE. The input vectors A_i^{IN1} and A_i^{IN2} are coded into the intensity spectrum of the first $I_1(\omega)$ and the second excitation pulse $I_2(\omega)$, respectively. The product $A_i^{OUT} = A_i^{IN1} \cdot A_i^{IN2}$ is coded into the echo spectrum $I_e(\omega)$.

6.2 FUTURE APPLICATIONS

As we see in figure 6.1, it is possible to store eight bits of information in the echo. How can our results be discussed with respect to possible applications in the future?

For example, by using a frequency detector which is able to measure in parallel the intensities at eight different frequencies and at a repetition rate in the order of kHz, it should be possible to use this spectrally modulated pulses to transfer digital data, i.e. in a computer.

Actual state of the art of regenerative amplified femtosecond laser systems is about 10 kHz. An other bottleneck is the repetition rate of the LCA. Our LCA has a maximum repetition rate of about 10 Hz. Other types of SLM's might be faster, i.e. an acousto-optical modulator, but these repetition rates are anyway far from that of the laser system.

With higher spectral resolution, it would be possible to store more bits in the echo spectrum. The information density could also be increased if the detector can distinguish between different intensities for any frequency component (bit), e.g. if it is able to detect zero, half-maximum and maximum intensity, which can be assigned to the bit information 0, 0.5 and 1 respectively.

7 REFERENCES

[ALL-87] L. Allen, J. H. Eberly, *Optical resonance and two-level atoms*, Dover, 1987.

[BLÜ-90] B. Blümich, *Echos in der Spectroscopie,* Chemie in unserer Zeit, 24. Jahrg. 1990, Nr. 1.

[BOY-92] R. W. Boyd, *Nonlinear Optics*, Academic Press, Inc., 1992.

[CLA-95] Clark-MXR Inc., *DT-505 Pockels Cell System User's manual,* version 2.2, 1995.

[GAL-96] J. Gallus, *Spectrale Modulation von Femtosekunden-Pulsen und Anwendung auf Zwei-Photonecho-Experimente*, Diplomarbeit ETH Zürich, 1995/96.

[KNE-95] F. K. Kneubühl, M. W. Sigrist, *Laser*, Teubner Studienbücher, Stuttgart, 1995.

[KOE-96] W. Koechner, *Solid-state laser engineering*, Springer-Verlag Berlin Heidelberg, 1996.

[KRÖ-96] S. Kröll, U. Elman, *Photon-echo-based logical processing*, Opt. Lett. 18, 1834, 1993.

[KRÖ-96] S. Kröll, *Anteckningar till kursen i Icke-linjär optik*, Lund, 1996.

[MAI-88] P. Maine, D. Strickland, P. Bado, M. Pessot, G. Mourou, *Generation of ultrahigh peak power pulses by chirped pulse amplification*, IEEE Journal of Quantum Electronics 24 (2), 398, 1988.

[MUK-95] S. Mukamel, *Nonlinear Optical Spectroscopy*, Oxford University Press, 1995.

[SAA-86] P. Saari, R. Kaarli, A. Rebane, Picosecond time- and space-domain holography by photochemical hole burning, J. Opt. Soc. Am. B, Vol. 3, No. 4, April 1986.

[SCH-94] H. Schwoerer, *Spektrale Lochbrennmaterialien als Hochauflösende lineare Amplituden- und Phasenfilter für ultra-kurze Laserpulse*, Diss. ETH Zürich Nr. 10933, 1994.

[WEF-95] M. Wefers, K. Nelson, *Analysis of programmable ultrshort waveform generation using liquid-crystal spatial light modulators*, J. Opt. Soc. Am. B 12, 7 (1995), 1343.

[YAR-89] A. Yariv, *Quantum Electronics*, John Wiley & sons, 3rd edition, 1989.

[ZUI-96] V. Zuikov, W. Ferri, O. Ollikainen, A. Rebane, U. P. Wild, *Wave Matching of Femtosecond and Picosecond Photon Echoes in Dye-doped Polymer Films*, Laser Physics, Vol 6, No. 4, pp. 729-734, 1996.